AD-A207 503 GROUND CLUTTER FILTERS FOR STAGGERED PULSE TRAINS(U) 1/1
NATIONAL OCEANIC AND ATMOSPHERIC ADMINISTRATION NORMAN
OK NAT S S ZRNIC' ET AL MAR 89 DOT/FAA/SA-89/2
UNCLASSIFIED DTFA01-80-Y-10524 F/G 17/9 NL

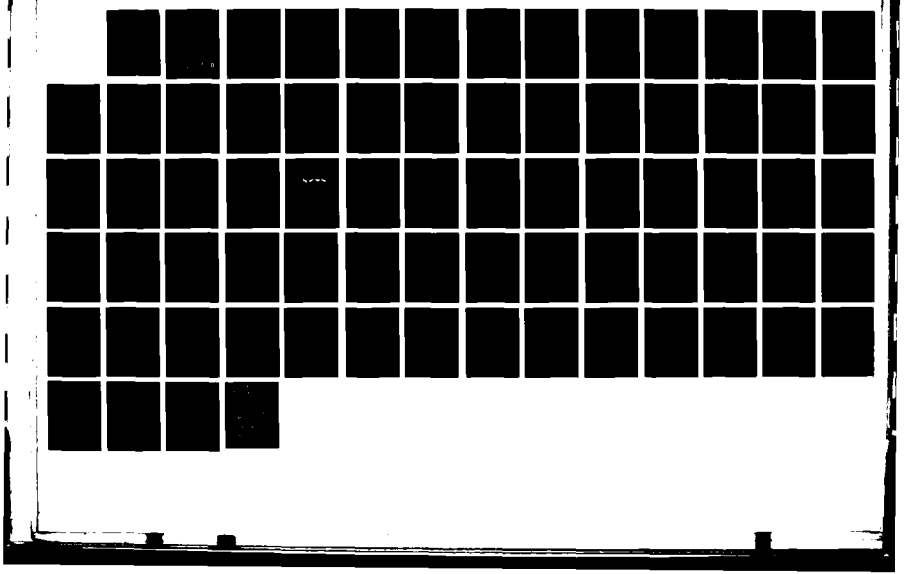

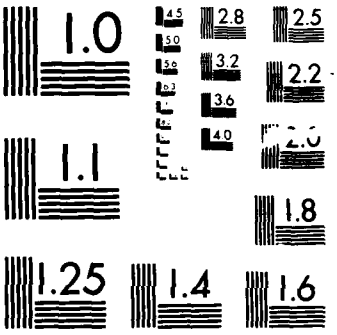

DOT/FAA/SA-89-2

Advanced System
Acquisition Service
Washington, D.C. 20591

Ground Clutter Filters for Staggered Pulse Trains

Dusan S. Zmic'
Zoran Banjanin
NOAA, Environmental Research Laboratories
National Severe Storms Laboratory
Norman, OK 73069

March 1989

Final Report

Technical Report Documentation Page

1. Report No.	2. Government Accession No.	3. Recipient's Catalog No.
DOT/FAA/SA-89/2		

4. Title and Subtitle	5. Report Date
Ground Clutter Filters for Staggered Pulse Trains	March 1989
	6. Performing Organization Code
	8. Performing Organization Report No.
7. Author(s)	
Dusan S. Zrnic' and Zoran Banjanin	MGG000
9. Performing Organization Name and Address	10. Work Unit No. (TRAIS)
National Severe Storms Laboratory 1313 Halley Circle Norman, OK 73069	11. Contract or Grant No. DTFA01-80-Y-10524
	13. Type of Report and Period Covered
12. Sponsoring Agency Name and Address	Final Report
U.S. Department of Transportation Federal Aviation Administration Advanced System Acquisition Service, ASA-1 Washington, DC 20591	14. Sponsoring Agency Code ASA-220

15. Supplementary Notes

16. Abstract

Several methods for canceling ground clutter on Doppler weather radars that operate with staggered PRT's are investigated. The scheme is developed that consists of two filters that operate sequentially, so that the overall filter is time-varying, with periodically changing coefficients. This filter is analyzed theoretically and through simulations for a stagger ratio of 3/2, which extends the unambiguous velocity interval (at a wavelength of 5 cm) to 50 m/s. The amplitude characteristic of the filter over this interval is very good, but the phase characteristic, which is nonlinear in about 40% of the interval, requires that a special decision logic be used for velocity estimation. At high signal-to-noise ratio (> 20 dB), mean velocities obtained from the output meet terminal Doppler weather radar specifications.

Keywords: Pulse Repetition Time; Next Generation weather radar;

17. Key Words	18. Distribution Statement
Weather; Radar; Doppler; NEXRAD; Ground Clutter;	This document is available to the public through the National Technical Information Service, Springfield, Virginia 22161

19. Security Classif. (of this report)	20. Security Classif. (of this page)	21. No. of Pages	22. Price
UNCLASSIFIED	UNCLASSIFIED	57	

Form DOT F 1700.7 (8-72) Reproduction of completed page authorized

PREFACE

The authors appreciate consultations with Jim Evans and Mark Goldberg. Bob Maddox, E. Chornoboy and N. Balakrishnan's review and help improved the report. Carole Holder typed the manuscript, and Joan Kimpel did the artwork.

TABLE OF CONTENTS

LIST OF FIGURES

Mathematical Notation

f	frequency
h_1, h_2	filter coefficients
$H(f)$	frequency response function
K	stagger ratio T_1/T_2
M	number of sample pairs
$\hat{R}$	autocovariance estimate
T_1, T_2	pulse repetition times (PRT)
$\hat{v}$	estimated velocity
v_c	cut-off velocity
v_m	unambiguous velocity
α	threshold level
δ	ripple in filter bands
ψ	phase characteristic
λ	wavelength
σ_c	clutter spectrum width
σ_s	signal spectrum width

Acronyms and Initialisms

CA	clutter attenuation
CGCF	comparative ground clutter filter
FIR	Finite Impulse Response Filter
GCF	ground clutter filter
LPF	Low-Pass Filter
NEXRAD	Next Generation Weather Radar
PRT	Pulse Repetition Time
SCR	signal-to-clutter ratio
SNR	signal-to-noise ratio
TDWR	Terminal Doppler Weather Radar

Ground Clutter Filters for Staggered Pulse Trains

Dusan S. Zrnic'
NOAA, Environmental Research Laboratories
National Severe Storms Laboratory
Norman, Oklahoma 73069

Zoran Banjanin
Cooperative Institute for Mesoscale Meteorological Studies,
University of Oklahoma
Norman, Oklahoma 73069

1. INTRODUCTION

A Doppler radar in the vicinity of airport terminals can provide timely information concerning weather hazards. The Next-Generation Weather Radar (NEXRAD), if properly sited, will have all the needed capability to serve that purpose. But because of its design to satisfy a multi-user mission, the NEXRAD may not be operated in modes that scan airport areas optimally, and moreover, there may be less than 35 NEXRADs in the vicinity of major airports. Therefore, the FAA is seriously considering a Terminal Doppler Weather Radar (TDWR), specifically for automatic detection and tracking of weather hazards within the terminal operations area of important aviation hubs. It has been well established that a 10 cm wavelength is preferable for storm surveillance (Doviak et al., 1978); however, at close range, a shorter wavelength (e.g., 5 cm) could be used at some cost savings. For the same beamwidth it is considerably simpler to achieve lower sidelobes at a 5 cm wavelength; similarly, a good radome is easier to build if the antenna is smaller, and waveguide and transmitter costs are lower. Besides, with a fixed antenna dish size, a 5 cm wavelength would produce a beamwidth half as wide as a 10 cm wavelength would, which would lead to a correspondingly better performance in ground clutter environment. Also, near major airports frequency allocation is not available at S band. Alas, the range and velocity ambiguities are twice as severe at 5 cm wavelength, and attenuation is much more significant. It is our belief that a uniform pulse repetition on a 5 cm weather radar would not be a choice waveform unless some phase encoding of pulses were utilized. In the absence of phase encoding, a staggered pulse sequence would need to be employed in order

to extend the unambiguous range and velocity. The study reported here examines ground clutter canceling on a staggered pulse sequence. Because TDWR's main mission is to observe weather at low altitudes, any realistic signal processing scheme must include a suitable canceler.

2. STAGGERED PRT

By suitably combining velocity or autocovariance estimates from two different pulse repetition times (PRT) T_1 and T_2, it is possible to increase the unambiguous velocity effectively. Sirmans et al. (1976) analyzed a scheme (Fig. 1) whereby two velocity estimates $\hat{v}_1$ and $\hat{v}_2$ are obtained from two autocovariance estimates $\hat{R}(T_1)$ and $\hat{R}(T_2)$. When aliasing occurs, it will affect the two velocity estimates differently because their Nyquist intervals are different. As long as the expected difference $E(\hat{v}_1-\hat{v}_2)$ is unambiguous, mean velocity aliases can be resolved. A similar scheme has been described by Doviak and Zrnic' (1984) and analyzed by Zrnic' and Mahapatra (1985). They proposed to estimate the velocity $\hat{v}$ from

$$\hat{v} = -\frac{\lambda}{4\pi(T_2-T_1)} \arg(\hat{R}_1\hat{R}_2^*) \qquad (1)$$

where λ is the wavelength. The autocovariance estimates $\hat{R}_1$ and $\hat{R}_2$ at time lags T_1 and T_2 would normally be obtained from several sample pair autocovariances to reduce statistical uncertainty. It can be seen from Eq. (1) that the velocity estimate $\hat{v}$ becomes ambiguous when the phase difference, $\arg \hat{R}_1-\arg \hat{R}_2$, exceeds $\pm\pi$. Therefore, a corresponding unambiguous velocity is defined by

$$v_m = \pm \frac{\lambda}{4(T_2-T_1)} = \pm \frac{\lambda}{4T_2(1-K)} = \pm \frac{\lambda}{4T_s} \qquad (2)$$

where $T_2 > T_1$, $K = T_1/T_2$, and $T_s = T_2-T_1$.

It follows from (2) that larger unambiguous velocities are obtained for smaller differences between T_2 and T_1. But the difference cannot be made too small because the errors in $\hat{v}$ due to statistical fluctuations (in estimates $\hat{R}_1$ and $\hat{R}_2$) are inversely proportional to this difference.

The normalized plot of the standard deviation is shown in Fig. 2. Signal-to-noise ratios (SNR) of 20 dB and 5 dB are used, K is a parameter, and $v_{a2} = \lambda/4T_2$. Our choice of a 20 dB SNR is motivated by the fact that at this and larger SNRs the standard errors of estimates are independent of SNR. For

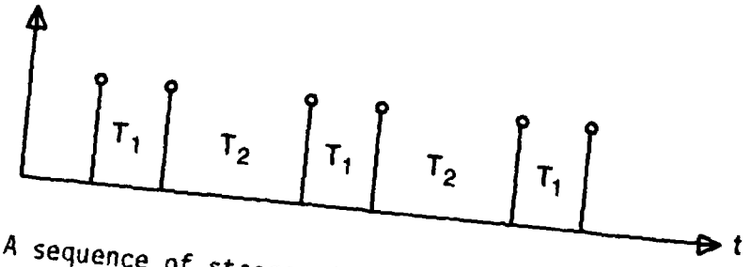

Figure 1. A sequence of staggered pulses.

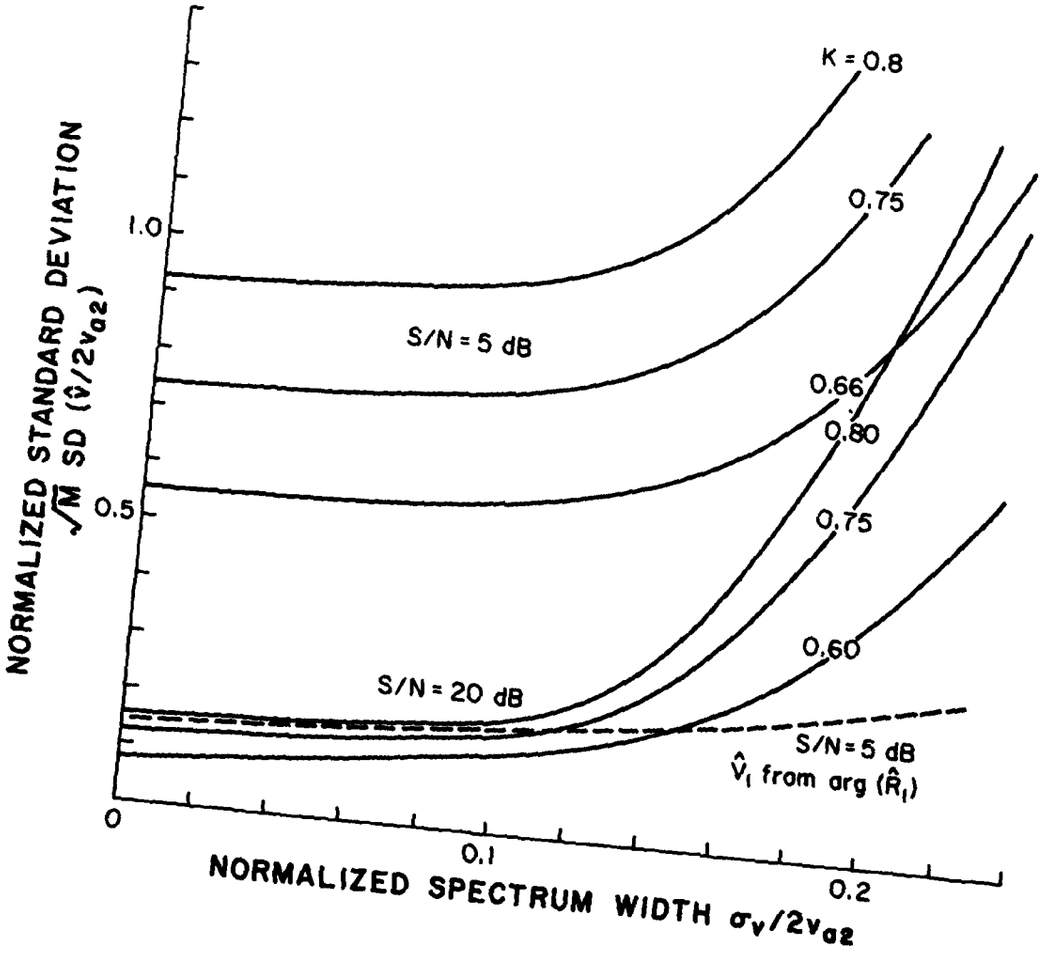

Figure 2. Normalized standard deviation of mean velocity estimates from staggered PRT scheme. The SNR is 5 dB for upper three curves, and 20 dB for lower solid curves; the dashed curve is the standard deviation of the estimated velocity $\hat{v}_1$, obtained from the argument of the autocovariance $\hat{R}_1$.

the same number of sample pairs, M, the standard errors are considerably larger than when contiguous or independent pairs are used (Zrnic', 1979). As a matter of fact, it seems that errors can be controlled only if the SNR is larger than 20 dB. This is usually the case when echoes originate from appreciable precipitation (equivalent reflectivity factor of 30 dBZ or more). Close to the radar a considerably smaller reflectivity factor can produce the large SNR; for the NSSL Doppler radar a 0 dBZ reflectivity factor at a 10 km range produces a 20 dB SNR.

As an example let us consider a 5 cm weather radar with T_2 = 1.5 m s and T_1 = 1 m s. The factor K = 0.66, and v_{a2} = 8.3 m s^{-1}. Now, if the spectrum width is 2 m s^{-1}, the normalized error from Fig. 2 becomes 0.15. Therefore a 1 m s^{-1} error in velocity estimates can be achieved with M=6 sample pairs. In severe storms, the median value of spectrum width is 4 m s^{-1} (Doviak and Zrnic', 1984), and also it is the value that may be produced by significant turbulence. With a spectrum width of 4 m s^{-1} we need 64 sample pairs to bring the error below 1 m s^{-1}.

The errors can be significantly reduced if the mean velocity is computed in a two-step process. First, an estimate $\hat{v}$ according to (1) having the extended unambiguous velocity v_m is found. Then a second estimate $\hat{v}_1$ from the autocovariance $\hat{R}_1$ is computed. This estimate has a much lower standard error than the first (Zrnic', 1977) and also a small unambiguous interval $2v_{a1} = \lambda/2T$. It suffices to add (subtract) multiples of $2v_{a1}$ to (from) $\hat{v}_1$ until the absolute difference $|\hat{v} - \hat{v}_1 - 2nv_{a1}|$ is minimized. Thus-found positive or negative integer n determines the new extended velocity estimate $\hat{v}_1 + 2nv_{a1}$, which now has the same standard error as $\hat{v}_1$ (unless catastrophic errors in $\hat{v}$ have occurred). To illustrate the point, let us return to our example with K = 0.66, v_{a1} = 12.5 m s^{-1}, v_{a2} = 8.3 m s^{-1}, and SNR = 5 dB. Furthermore, let us assume that there are 20 staggered pulses (M = 10 pairs), which is also the number we use later in our simulations. For a representative spectrum width of 2 m s^{-1} we find the standard deviation of $\hat{v}$ (from Fig. 2) to be 3.2 m s^{-1}, which is small enough, compared with $2v_{a2}$ = 16.6 m s^{-1}, to ensure that catastrophic errors (i.e., errors that yield wrong n) would seldom occur. The standard error of $\hat{v}_1$ (from the argument of $\hat{R}_1$) is also plotted in Fig. 2, according to the equations of Zrnic' (1977), and is normalized to $2v_{a2}$. Thus from the dashed curve, we compute the error in $\hat{v}_1$ to be about 1 m s^{-1}; this will also be the error in the dealiased velocity, provided no catastrophic

failure has occurred. For the example considered it can be shown by simulation (Chernoboy, 1988) that the catastropic errors would occur about 10% of the time. In our analysis we use the estimator (1), whose performance with respect to biases in the presence of clutter filters is indistinguishable from the more complicated two-step estimator. We must bear in mind that a practical implementation may require the two-step process, or averaging of velocities in range, in order to keep statistical errors under control.

Therefore, at close range (<30 km), which is of prime concern for the terminal Doppler radar, a staggered PRT would produce reliable estimates of velocities. These can be obtained at sufficiently high rates to make them useful for detection of short-lived transient weather phenomena such as microbursts. For the cited example, the extended maximum unambiguous velocity is $v_m = 25$ m s^{-1}. The shorter unambiguous range (corresponding to $T_1 = 1$ m s) is 150 km, and because pulses are staggered, overlaid echoes in range would not bias velocity estimates but would act like white noise to increase the standard error. It is evident that this staggered PRT scheme can make a radar with a 5 cm wavelength perform much like a 10 cm radar, as far as ambiguities are concerned. But at close range in airport environments, ground clutter is of major concern, and staggered schemes do not lend themselves easily to clutter canceling.

3. GROUND CLUTTER FILTER

Ground clutter filters (GCF) with sharp narrow notches (50 dB deep and 1-2 m s^{-1} wide) can easily be designed to operate on uniformly spaced pulse trains. A comprehensive report by Zrnic' and Hamidi (1981) describes an infinite impulse response filter that meets these objectives. Ground clutter cancellation in the context of NEXRAD, and a finite impulse response filter that also achieves the objectives have been treated by Evans (1983). We shall show that filters can be designed to operate on staggered pulse trains and still meet the notch objective, yet the compromises introduced in a passband may be objectionable. In order to be useful, the filter must have a linear phase characteristic over most of the band so that the phases of R_1 and R_2 are linear leading to unbiased Doppler estimates (1). A reasonably flat amplitude characteristic is needed to avoid biases of the spectreal moments.

Four approaches to filter design are examined in the sequel. All require dwell times of the order of the reciprocal of the filter notch width. The

four are based on using (1) a pair of filters each for a low uniform PRT, (2) a high, uniform interpolated PRT, (3) staggered pulses, and (4) a comparative ground clutter filter that uses both split uniform and staggered pulses.

3.1 A Pair of Clutter Filters Each for a Uniform Pulse Repetition Time (PRT)

One very simple method for preserving linear phase of the Finite Impulse Response (FIR) filters, in the case of nonuniform sampling, is shown in Fig. 3. Through the remainder of the report we call this realization the split uniform PRT ground clutter filter. The input time series, with nonuniformly spaced samples, is divided into two time series with uniformly spaced samples, each of which is processed by two independent ground clutter filters. These filters can be designed using methods developed by Rabiner and Gold (1975). The phase characteristic of this composite system can be linear, if each ground clutter filter has such a characteristic. But the amplitude characteristic has notches not only at zero frequency, but also at

$$f_n = n/T,\ T = T_1+T_2,\ n = 0, \pm1, \pm2, \pm3, \qquad (3)$$

because the sampling frequency is T^{-1}. For T_1 = 1 ms and T_2 = 1.5 ms this corresponds to notches at velocities of ±10 m s^{-1}, ±20 m s^{-1}, ±30 m s^{-1}, etc., in addition to the desirable notch at 0 velocity (Fig. 4). If each notch were 2 m s^{-1} wide, about 16% of the unambiguous velocity interval ($2\ v_m$ = 50 m s^{-1}) would be effectively eliminated from measurements in addition to a 4% notch, at zero velocity. This may be a large price to pay for clutter canceling.

In summary, a pair of finite impulse response filters can be designed to have a linear phase characteristic so that there would be no phase contamination of the autocovariance estimates $\hat{R}_1$ and $\hat{R}_2$. But the amplitude characteristic would have periodic notches that would preclude measurements of weather echoes in a considerable percentage of the extended unambiguous interval.

3.2 Filter that Operates on a Train of Interpolated High-PRT Pulses

We consider here interpolation in a staggered PRT train of pulses so that the resulting PRT becomes uniform. Such interpolation is fairly simple if the stagger ratio K is a ratio of two small integers such as 2/3 or 3/4. For instance, for K = 2/3, it suffices to interpolate one value in a T_1 interval and

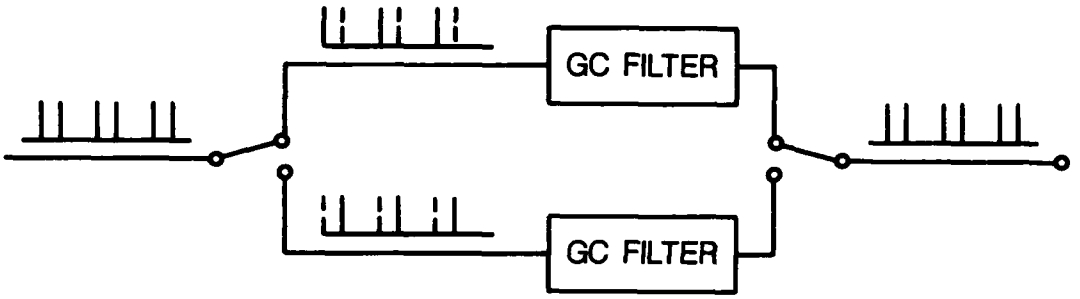

Figure 3. Ground clutter filter consisting of a pair of filters, each of which is for a low-PRT uniform pulse train. This pair is referred to as the split uniform PRT ground clutter filter.

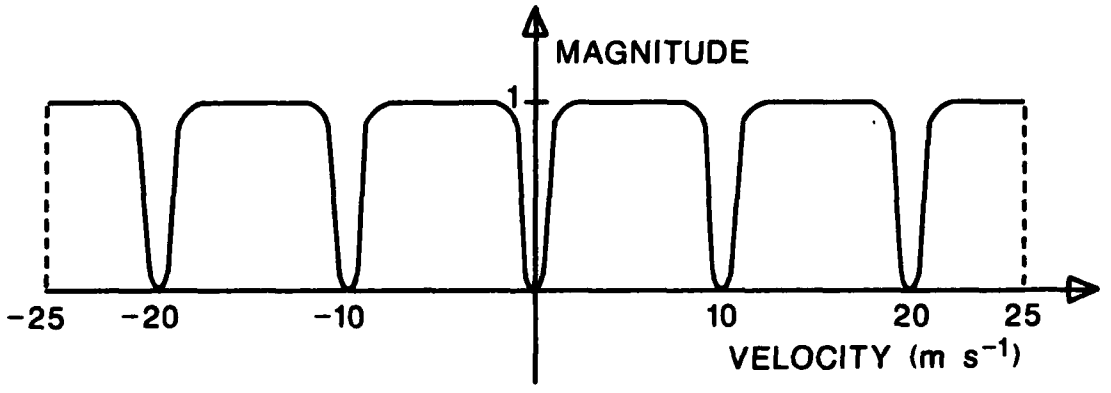

Figure 4. Sketch of a transfer characteristic produced by one filter of the pair in Fig. 3. The example assumes T_1 = 1 ms, T_2 = 1.5 ms, and λ = 5 cm so that the extended unambiguous velocity v_m = 25 m s^{-1}.

two values in a T_2 interval (Fig. 5a). But there may be advantages in using a different interpolation scheme. In Fig. 5b the interpolated pulse train is such that one of the original pulses is not passed to the filter, and therefore, after the filter, another interpolation is needed to restore the sample spaced by T_1. Finite impulse response filters can be used to filter the ground clutter, but as in the previous example, aliasing of velocities will adversely affect the weather echoes in the passband. Although the exact analysis of aliasing can be complicated, a heuristic approach that gives, on the average, a correct result, is very simple. It is known that in a pulse train with a random PRT, aliasing will occur, on the average, for frequency components that exceed $(1/2T_a)$ where T_a is the average PRT in the sequence. If we accept that the same holds true for a staggered PRT, we recognize that on the average, aliasing will occur at $1/(T_1+T_2)$. This means that a notch at DC will also repeat, on the average, at $\lambda/2T$ intervals. For our example of v_m = 25 m s^{-1}, T = 2.5 ms, and λ = 5 cm, this is illustrated in Fig. 6 where dashed notches indicate degradations of the amplitude characteristic. However, these interpolation schemes generally distort the phase, causing serious biases in estimates (1). If the notch is 2 m s^{-1} wide, we see that about 16% of the 50 m s^{-1} velocity interval is now lost for processing. Although such a loss may be acceptable, we emphasize that we have yet to demonstrate that a filter can be designed to perform according to the above theory. We also need to determine which of the two interpolation schemes illustrated in Fig. 5 is best suited for clutter filtering, and furthermore, a method to overcome phase distortions must be devised!

3.3 Filter that Operates on Staggered Pulses

A diagram of a filter that operates on a staggered pulse train is shown in Fig. 7. The diagram illustrates the design philosophy, and it need not be construed that the actual implementation should follow the same flow path. As we shall see later, there are implementations that save computation by combining several steps from our diagram. In this diagram the staggered pulse train is split. One path contains a low-pass filter to retrieve the ground clutter component. The low-pass filter is an FIR filter that contains two sets of coefficients, which are alternately active. Filter coefficients are chosen in such a way that the filtered values are actually interpolated into a uniform pulse train. Thus, there are no phase distortions at the output of the

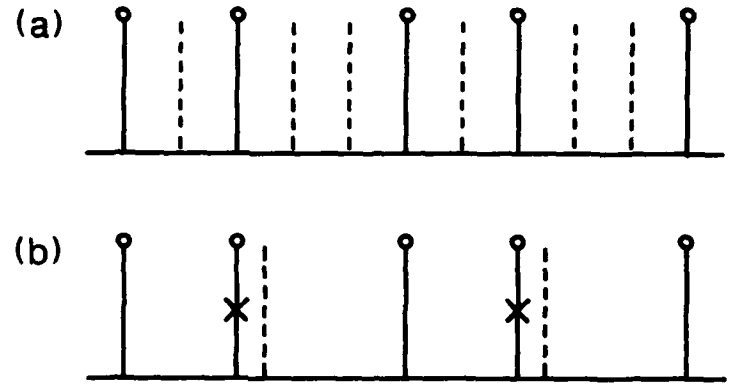

Figure 5. (a) Interpolated pulse train for K = 2/3.
(b) Minimal interpolation to obtain a uniform pulse train.

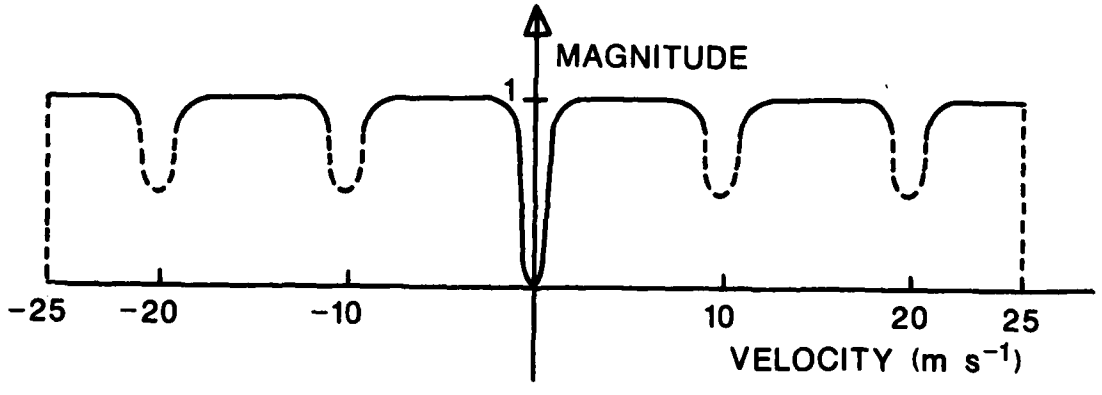

Figure 6. Position of notches produced by a clutter filter on interpolated pulses.

GROUND CLUTTER FILTERING

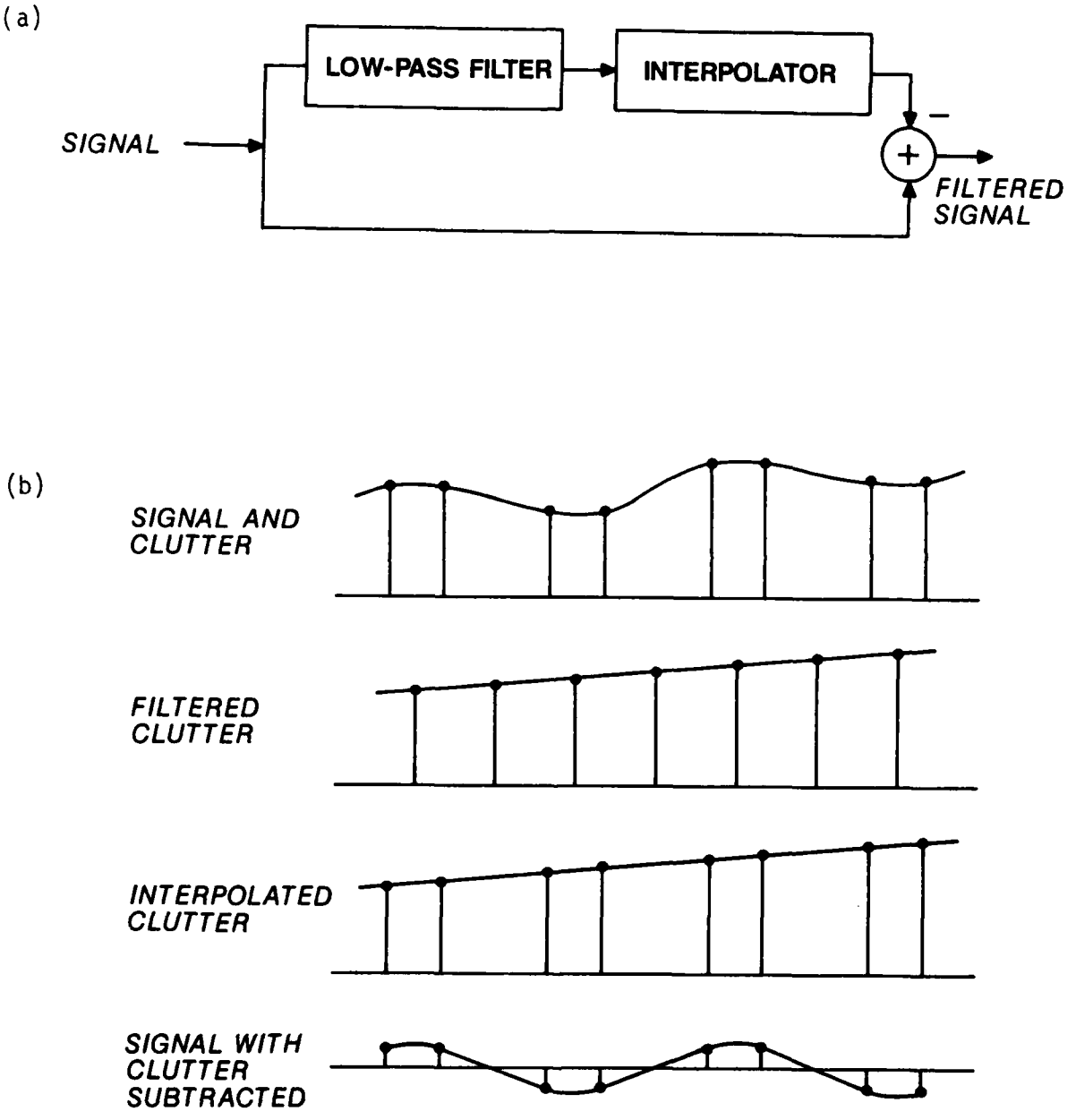

Figure 7. (a) Block diagram of a filter for staggered pulses.
(b) Pictorial representation of the filtering process in (a).

low-pass filter. The interpolator interpolates the uniform pulse train back into a staggered pulse train so that proper subtraction can be realized, after which most of the ground clutter would be removed, as shown in Fig. 7. There are some small differences in the analysis when even or odd numbers of samples are filtered, and we shall treat the two cases separately.

3.3.1 Even number of samples

The center of symmetry of the weighting coefficients is in the middle of either T_1 or T_2, and it switches periodically between the two with each new pulse (Fig. 8a).

The impulse response functions for the two sets of low-pass filter coefficients will be denoted with $h_1(u)$ and $h_2(\tau)$; in this notation we assume that the coefficients are centered on T_1 and T_2 and that $u = t + T_1/2$ and $\tau = t - T_2/2$. Thus, the frequency responses $H_1(f)$ and $H_2(f)$ are real functions. In order to account for the time displacement between the action of the two filters (Fig. 8a) we must introduce appropriate phase factors, so that the frequency responses taken together become

$$H_1'(f) = H_1(f)\, e^{j\omega T_1/2}$$
$$H_2'(f) = H_2(f)\, e^{-j\omega T_2/2} \qquad (4a)$$

where

$$H_1(f) = \sum_{i=-n}^{n} h_1(u_i)\, e^{-j\omega u_i}$$
$$H_2(f) = \sum_{i=-n}^{n} h_2(\tau_i)\, e^{-j\omega \tau_i}. \qquad (4b)$$

The dependent variables u_i and τ_i are used to indicate that the weighting coefficients h_1 and h_2 are never coincident in time, and furthermore, u and τ axes are displaced from the reference time axis as in Fig. 8a.

Because the low-pass filters H_1 and H_2 select the ground clutter, the shape of the notch will depend on the passband characteristic of H_1 and H_2. Obviously, it is desirable to match H_1 and H_2 to the clutter spectrum and to suppress all the components outside the interval containing clutter. Ideally, H_1 and H_2 should have identical frequency behavior. This can be accomplished approximately if h_1 and h_2 are obtained from the same continuous window function. In the sequel we use the Hamming window, as well as more sophisticated

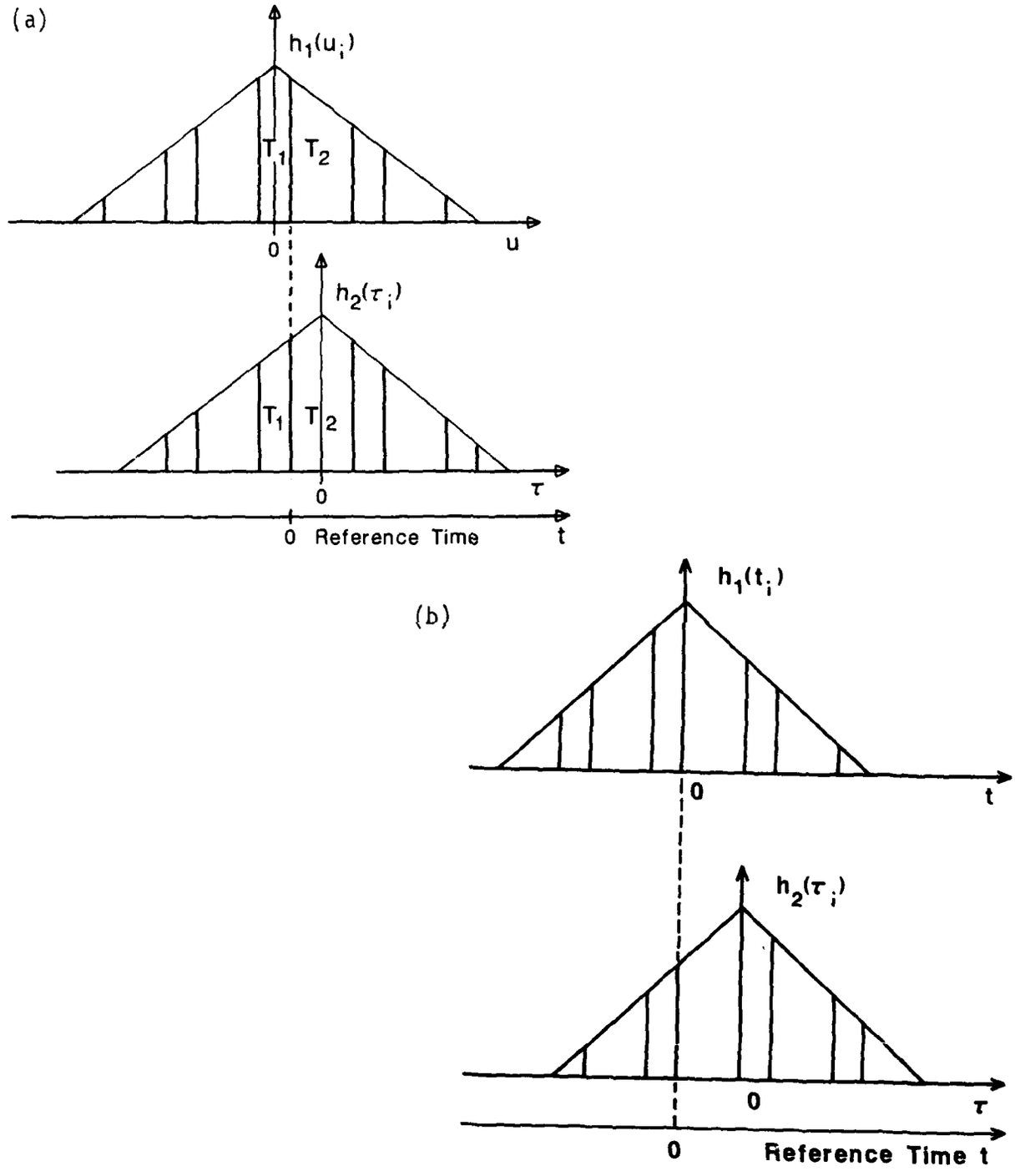

Figure 8. (a) Representation of the weighting by h_1 and h_2 corresponding to a transfer H_{s1} and even number of samples.

(b) Representation of the weighting by h_1 and h_2 corresponding to a transfer H_{s1} and odd number of samples.

windows, to determine the coefficients $h_1(u_i)$ and $h_2(\tau_i)$. Because the Hamming window has spectral skirts about 45 dB below the main lobe peak, the overall high-pass filter frequency response would resemble the one suggested for NEXRAD.

At the output of low-pass filter, the pulses have equal spacings and they must be interpolated back to a staggered train, so that proper subtraction and later computation of autocovariances can be made. We chose a simple linear interpolation so that outputs of filter H_1 are multiplied by a constant A, and of H_2 by a constant B; the two products are summed and subtracted from the total signal. In this manner the overall transfer function of the system (Fig. 9) becomes

$$H_{s1}(f) = 1 - A\, H_1(f)\, e^{j\omega T_1/2} - B\, H_2(f)\, e^{-j\omega T_2/2} \qquad (5a)$$

where A+B = 1. The coefficients A and B determine the relative contributions of the two outputs (h_1 and h_2) to the interpolated value. For common stagger ratios (2/3) the weight would be 3/5 and 2/5, but it is our experience that A = B = 0.5 works as well, and the value will be used throughout this report. For illustration, we will also set one of these coefficients to zero.

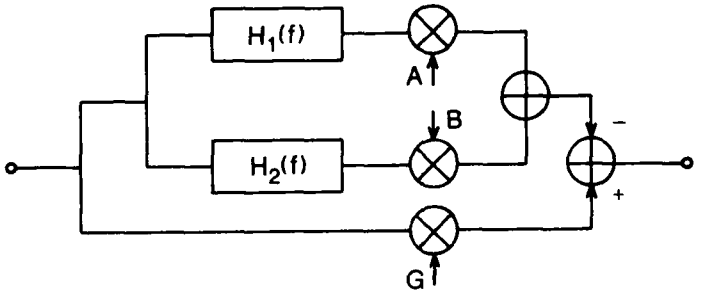

Figure 9. A more detailed block diagram of the staggered PRT ground clutter filter represented in Fig. 8.

Note that the transfer (5a) is valid for the arrangement of the staggered pulse train as in Fig. 8a (i.e., the interpolation is at t=0). For the next interpolated pulse the exponential terms in (5a) would change sign to produce

$$H_{s2}(f) = 1 - A\, H_1(f)\, e^{-j\omega T_1/2} - B\, H_2(f)\, e^{+j\omega T_2/2}. \qquad (5b)$$

The pair, (5a) and (5b), constitutes a time-varying filter that cycles through two transfer functions at the rate of 1/T. Our design matches the magnitudes of the transfer functions so that there are no amplitude modulations due to this cycling. However, as we shall see in the later example, there is a phase modulation in several very narrow frequency bands and these must be dealt with.

3.3.2 Odd number of samples

In this case the coefficients $h_1(t_i)$ and $h_2(\tau_i)$ (Fig. 8b) are not symmetric and corresponding frequency responses $H_1(f)$ and $H_2(f)$ are not real functions. But the weighting coefficients h_1 and h_2 have an odd symmetry with respect to each other [$h_1(-t_i) = h_2(\tau_i)$, see Fig. 8b]. Again to account for the time displacement between the action of the two filters (Fig. 8b) we must introduce appropriate phase factors, so that the frequency responses taken together become

$$\begin{aligned} H_1'(f) &= H_1(f) \\ H_2'(f) &= H_2(f)\, e^{-j\omega T_2} \end{aligned} \qquad (6a)$$

where

$$\begin{aligned} H_1(f) &= \sum_{i=-n}^{n} h_1(t_i)\, e^{-j\omega t_i} \\ H_2(f) &= \sum_{i=-n}^{n} h_2(\tau_i)\, e^{-j\omega \tau_i}. \end{aligned} \qquad (6b)$$

The variables t_i and τ_i are used to indicate that the weights h_1 and h_2 are never coincident in time. As in the previous case, the overall transfer function of the system becomes

$$H_{s1}(f) = 1 - A \cdot H_1(f) - B \cdot H_2(f)\, e^{-j\omega T_2}, \qquad (7a)$$

where A+B = 1. The transfer (7a) is valid for the arrangement of the staggered pulse train as in Fig. 8b. For the next interpolated pulse the transfer is

$$H_{s2}(f) = 1-A \cdot H_1(f)\, e^{-j\omega T_1} - B \cdot H_2(f). \qquad (7b)$$

Together, equations (7a) and (7b) constitutes a time-varying filter that cycles at the rate of 1/T.

3.3.3 Alternate realization of the filter

The hardware realization shown in Fig. 9 can be simplified by appropriately combining the h_1 and h_2 filter coefficients. Figure 10 illustrates how this can be done, so that the equivalent (to Eq. 5) high-pass coefficients become

$$\begin{aligned}
h_{s1}(t_n) &= -A \cdot h_1(\mu_n) \\
h_{s1}(t_{n-1}) &= -A \cdot h_1(\mu_{n-1}) - Bh_2(\tau_n) \\
&\vdots \\
h_{s1}(t_o) &= G-A \cdot h_1(\mu_{-1}) - Bh_2(\tau_1) \\
&\vdots \\
h_{s1}(t_{-n+1}) &= -A \cdot h_1(\mu_{-n}) - Bh_2(\tau_{-n+1}) \\
h_{s1}(t_{-n}) &= -Bh_2(\tau_{-n})
\end{aligned} \qquad (8)$$

At this point we stress that the compact realization as in Fig. 10 may not be the most desirable because, as we shall see later, there may be a need to obtain certain summations that are identifiable as parts of the low-pass filters. This may be necessary in order to resolve phases when signal velocities are at frequencies ±1/T, ±2/T, etc., where a large uncertainty in phase occurs. It is interesting to notice that although initially the two low-pass filters had an even number of samples after this hardware simplification, we have obtained one filter with an odd number of samples.

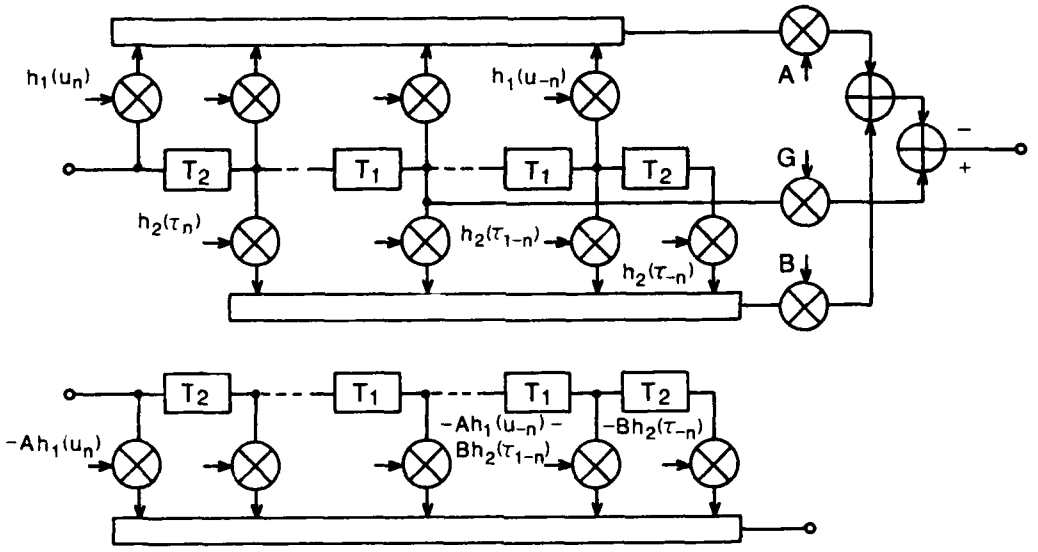

Figure 10. A schematic showing how the filter structure can be reduced to an equivalent high-pass filter with one set of coefficients.

Example 1

In the example that follows we use 40 pulses, T_1 = 1 ms, T_2 = 1.5 ms, and for simplicity, the weighting function for the low-pass parts, h_1 and h_2, is Hamming. The low-pass transfer function

$$AH_1(t)e^{j\omega T_1/2} + BH_2(t)e^{-j\omega T_2/2}$$

is plotted in Fig. 11 where we note the enhanced peaks at f = 1/T, 2/T, etc., or 10 m s^{-1}, 20 m s^{-1}, etc. As we shall see shortly, this is precisely where the phase characteristic has problems. In Fig. 12 we show the magnitude of the overall transfer function; both a normalized frequency $f(T_1+T_2)/2$ and velocity scale (for λ = 5 cm) are labeled. This characteristic is satisfactory; there is almost no attenuation at f = 1/T; small attenuation at f = 2/T can certainly be tolerated.

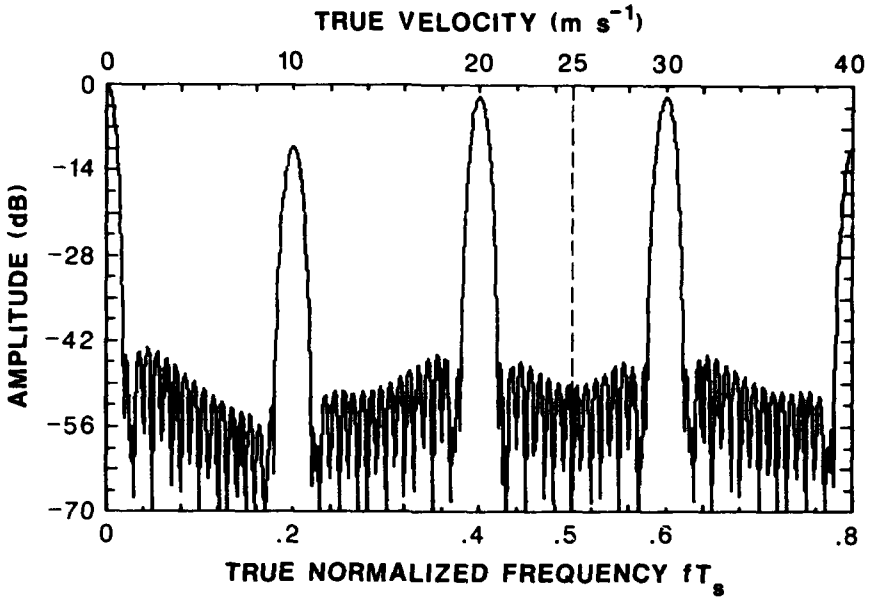

Figure 11. Magnitude characteristic of the low-pass portion of the filter. In this example A = B, K = 3/2, and Hamming weights are used.

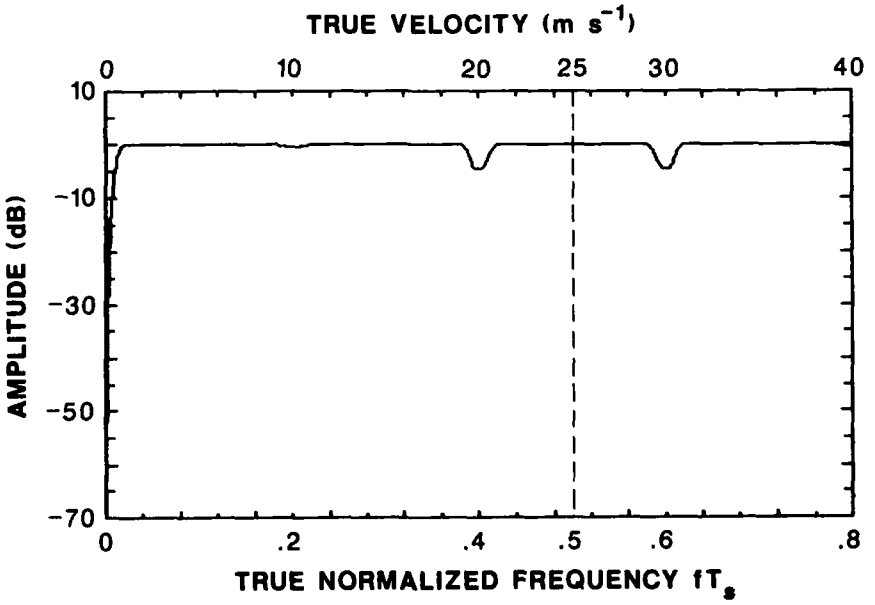

Figure 12. Magnitude of the overall transfer function (H_{s1} or H_{s2}).

The phase characteristics in Fig. 13a and b are for two positions of the pulse train (Eqs. 5a and 5b). Through most of the region the characteristic is flat, but at $f = \pm 1/T, \pm 2/T$, etc., there is a significant departure from the straight line. This departure cannot be tolerated because it would contaminate the autocovariance arguments. Because the phase shift alternates from pulse to pulse, it would add $2\psi(f)$ to the argument of the autocovariance R_1, and $-2\psi(f)$ to the argument of R_2 where $\psi(f)$ is the phase characteristic. Therefore, the added phase in Eq. (1) would be $4\psi(f)$. Obviously this would produce large errors in velocity estimates whenever $v = n\lambda/2T$, $n = \pm 1, \pm 2$, etc.

In Fig. 13c we have plotted the estimated versus true normalized Doppler frequency. The estimated is defined as $fT_2(1-K) + 4\psi(f)$, and the true is $fT_2(1-K)$; in the example $K=2/3$. Although this transfer looks discouraging, there are ways to identify situations when $fT_2/3 = \pm 0, \pm 0.2, \pm 0.4$, etc. This is discussed in Section 3.5.

3.4 General Design Procedure

In several approaches to the design of GCF which have been considered, most of the efforts have been devoted to the goal of achieving linear amplitude and phase characteristics in a passband. Now we turn our attention to the problem of achieving the desired stopband characteristic. Unlike the passband characteristic, which influences spectral parameter estimation, the stopband characteristic defines how well clutter is going to be attenuated.

The designing procedure is described in Fig. 14. In this figure, and throughout the rest of this report, we utilize a low-pass filter with an odd number of samples. The GCF is actually a high-pass filter, but the design procedure begins with a low-pass filter. The lower branch (direct connection) in Fig. 14 defines linear amplitude and phase characteristic of the GCF in the passband because the impedance of upper branch is very large at higher frequencies. This is generally true in the passband; however, at $f=0, \pm 1/T, \pm 2T$, etc. ($T_1 + T_2 = T$) there is a significant departure from constant amplitude and linear phase (Figs. 12 and 13).

The weighting function of a staggered PRT filter can be obtained from a uniform PRT filter that has a shorter sampling period T_u such that

$$T_u = T_1/n_1 = T_2/n_2$$

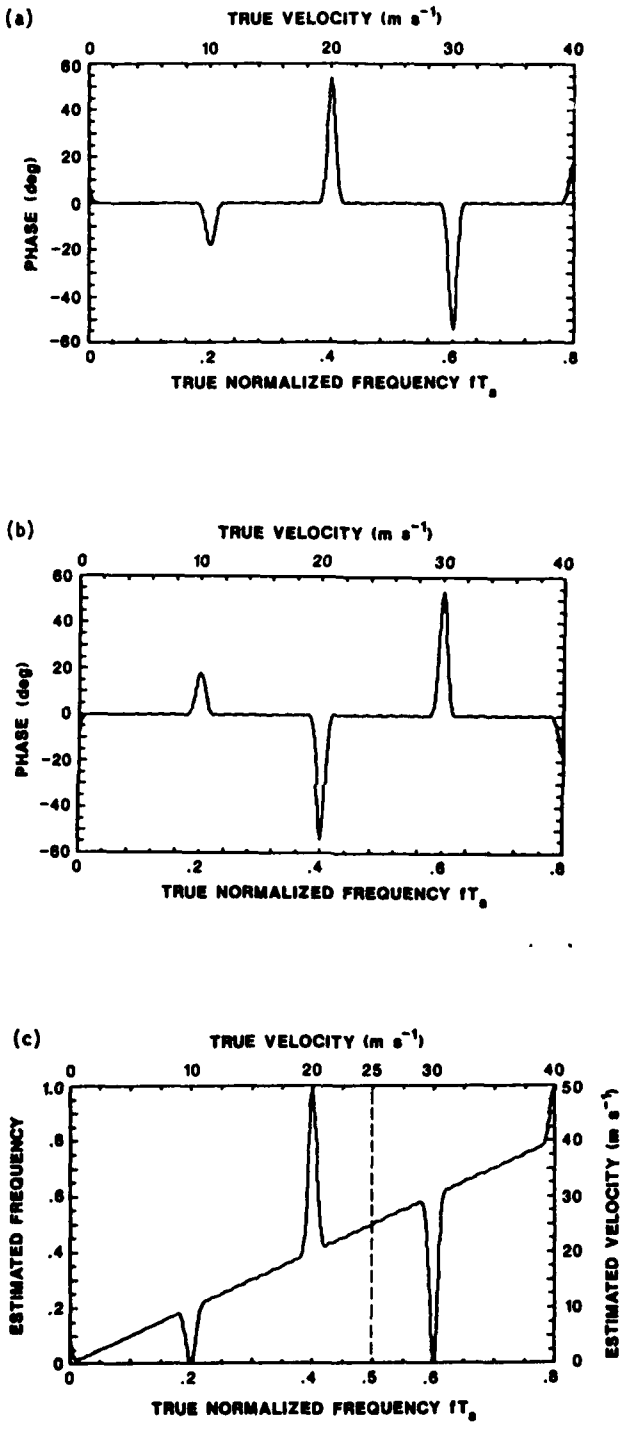

Figure 13. (a) Phase characteristic of the overall transfer function (H_{s1}).
(b) Phase characteristic of the overall transfer function (H_{s2}).
(c) Velocity transfer characteristic. The extended unambiguous velocity v_m = 25 m s^{-1}.

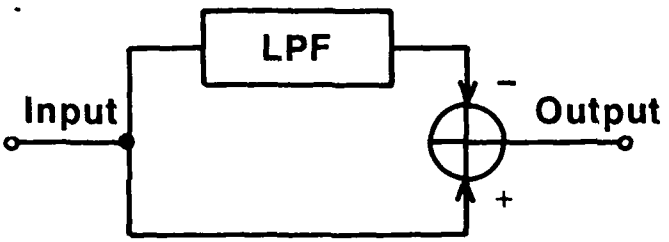

Figure 14. Diagram of GCF.

where n_1 and n_2 are prime integers that satisfy

$$K = T_1/T_2 = n_1/n_2.$$

This is accomplished by retaining only the weights that correspond to staggered spacings T_1 and T_2.

The transfer characteristic of the upper branch can be calculated as a function of staggered sampling times $t_i = 0, T_1, T, T + T_1, 2T$, etc.:

$$H(\omega) = \sum_{i=-\infty}^{+\infty} h(t_i)e^{-j\omega t_i} =$$

$$= \sum_{i=-\infty}^{+\infty} h(iT)e^{-j\omega iT} + \sum_{i=-\infty}^{+\infty} h(iT + T_1)e^{-j\omega(iT+T_1)} = \tag{10}$$

$$= H_1(\omega) + H_2(\omega)\, e^{-j\omega T_1},$$

where

$$H_1(\omega) = \sum_{i=-\infty}^{+\infty} h(iT)e^{-j\omega iT} \tag{11}$$

and

$$H_2(\omega) = \sum_{i=-\infty}^{+\infty} h(iT + T_1)e^{-j\omega iT} \tag{12}$$

are low-pass filters with a sampling period $T = T_1 + T_2$. If properly designed, the magnitudes of these two transfer functions would be almost identical, and if it were not for the term $e^{-j\omega T_1}$, the overall transfer would have identical peaks spaced at n/T. But because of complex addition, the peaks have varying amplitudes and associated phase shift (Figs. 11 and 12).

3.4.1 Design examples

The low-pass filter in the upper branch in Fig. 14 can be designed by modifying methods applicable to FIR digital filters with uniform sampling (Rabiner and Gold, 1975). Of these, we consider the optimal method (in the Chebyshev sense) and the window method.

Optimal filter design (Chebyshev) method

By considering the design problem as a Chebyshev approximation, it is possible to prove that this solution is optimal in a sense that the peak approximation error over the entire interval of approximation is minimized. There are several slightly different optional methods, but the one based on the Remez algorithm (Rabiner and Gold, 1975) has found the widest application.

Example 2

In the example that follows we use 101 uniformly spaced pulses, $T_u = T_s = 0.5$ ms, $T_1 = 1$ ms, and $T_2 = 1.5$ ms, $n_1 = 2$, $n_2 = 3$, and a software package DFDP (1985) for designing optimal filters to obtain LPF with $f_{c1} = 0.015$, $\delta_1 = 0.001$, $f_{c2} = 0.04$, and $\delta_2 = 0.03$ (f_{c1}, δ_1 are cutoff frequency normalized to the Nyquist interval and ripple in stopband, and f_{c2}, δ_2 are cutoff frequency and ripple in passband).

After all 101 weighting coefficients are applied (Fig. 14), the overall transfer characteristic of the GCF is as given in Fig. 15a. It is important to bear in mind that 101 uniform samples are not available and that the transfer characteristic shown serves only as a reference, to be compared with the transfer characteristic of the filter with staggered (sparse) coefficients. This is illustrated in Fig. 5a where dashed and solid samples together denote a uniform train and the solid samples by themselves are a stagger train of pulses. Transfer characteristic corresponding to the staggered case is shown in Fig. 15b. It is apparent that there are significant increases of the ripples in both passband and stopband, but they still retain the minimax property. Also, there are bands of increased attenuation around frequencies f = 1/T, 2/T, owing to staggered sampling.

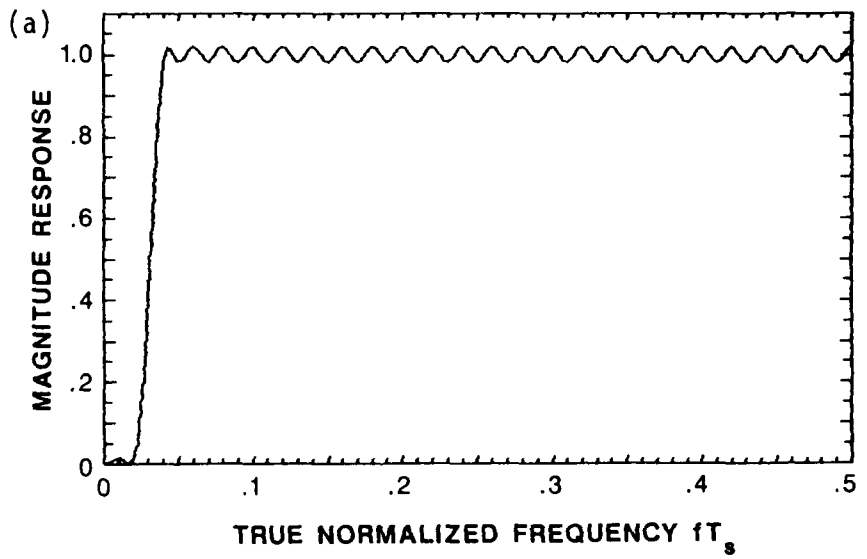

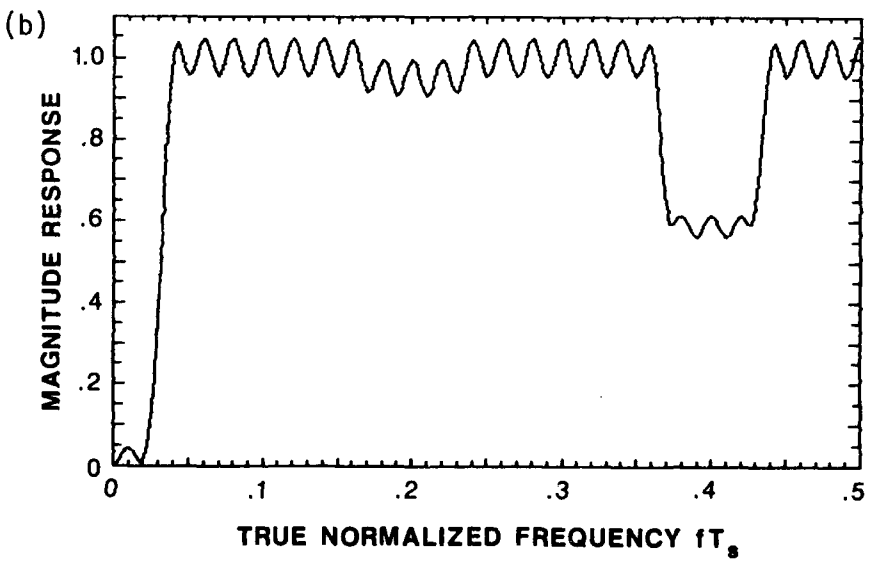

Figure 15. (a) Transfer characteristic of the Chebyshev GCF with 101 uniformly spaced coefficients; stopband cutoff frequency is 0.015, and passband cutoff frequency is 0.04.

(b) Transfer characteristic of the Chebyshev GCF with 41 staggered coefficients obtained from (a).

As performance measure of the GCF we use Clutter Attenuation (CA). This parameter is defined as the ratio of clutter power at the input to the power at the output of the clutter filter. It is assumed that ground clutter is well modeled by a narrow-band Gaussian process, which has a Gaussian spectral shape of variable width σ_c. We have integrated the product of the clutter spectrum and the power transfer function of the filter to obtain the output power. Figure 16 gives CA of both filters. Significant decrease of CA due to staggering is obvious.

Window filter design method

The most straightforward approach to FIR filter design is to truncate a desired infinite-duration impulse response sequence. An ideal desired frequency response is

$$H_o(e^{j\omega}) = \sum_{n=-\infty}^{\infty} h_o(n)e^{-j\omega n}, \tag{13}$$

where $h_o(n)$ is the corresponding impulse response sequence; i.e.,

$$h_o(n) = \frac{1}{2\pi}\int_{-\pi}^{\pi} H_o(e^{j\omega})e^{j\omega n}d\omega. \tag{14}$$

The finite length impulse response sequence h(n) can be represented as the product of the desired impulse response and a finite-duration "window" w(n):

$$h(n) = h_o(n)\cdot w(n). \tag{15}$$

The simplest window is a rectangular window:

$$w(n) = \begin{cases} 1, & 0 \leq n \leq N-1 \\ 0, & \text{otherwise} \end{cases}. \tag{16}$$

There are various windows, each of which offers a compromise between the width of the main lobe and the levels of sidelobes.

Let us consider next a window design of an LPF. The desired frequency response is

$$H_o(e^{j\omega}) = \begin{cases} 1, & |\omega| < \omega_c \\ 0, & \text{otherwise} \end{cases}; \tag{17}$$

the corresponding impulse response is

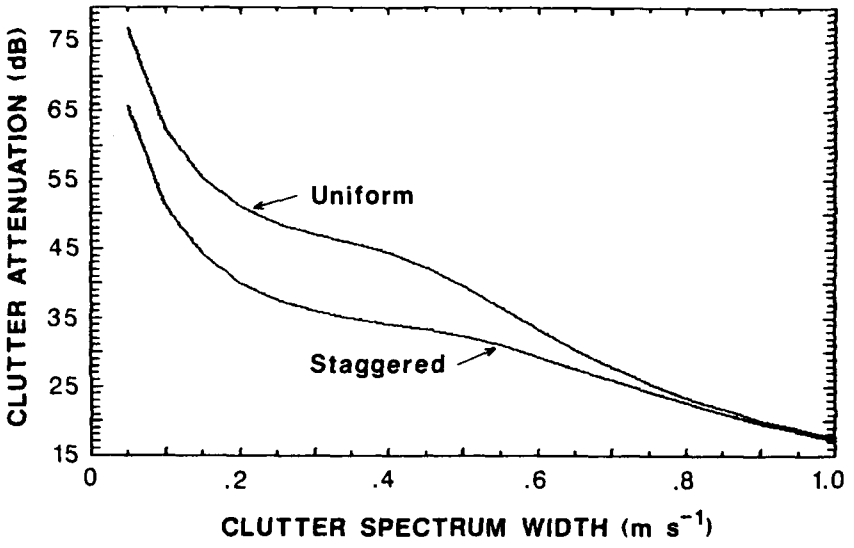

Figure 16. Clutter attenuation vs. clutter spectrum width (Chebyshev design) of the GCF with 101 uniformly spaced coefficients (upper curve) and GCF with 41 staggered coefficients (lower curve).

$$h_o(n) = \frac{\sin(2\pi f_c n)}{\pi n}, \tag{18}$$

and h(n) can be calculated from (15).

Example 3

As in the previous example, we take 101 pulses, T_1 = 1 ms, and T_2 = 1.5 ms (n_1 = 2, n_2 = 3). We use a Hamming window for w(n), and Eqs. (15) and (18) to design a filter with cutoff velocity v_c = 1.5 m s^{-1} ($f_c T_s$ = 0.03).

The overall transfer characteristic of the GCF with 101 uniformly spaced coefficients is given in Fig. 17a. Figure 17b shows the transfer characteristic corresponding to 41 staggered coefficients that span the same dwell time and are a subset of uniformly spaced coefficients. It is obvious that there is no deterioration of the stopband characteristic for the filter with staggered coefficients. However, there are bands of attenuation around frequencies f = 1/T, 2/T.

It is interesting to note that the transfer characteristic (Fig. 17c) of the split uniform PRT filter with 21 coefficients, which corresponds to the filter explained in Section 3.1, has a very similar shape of the notch. The

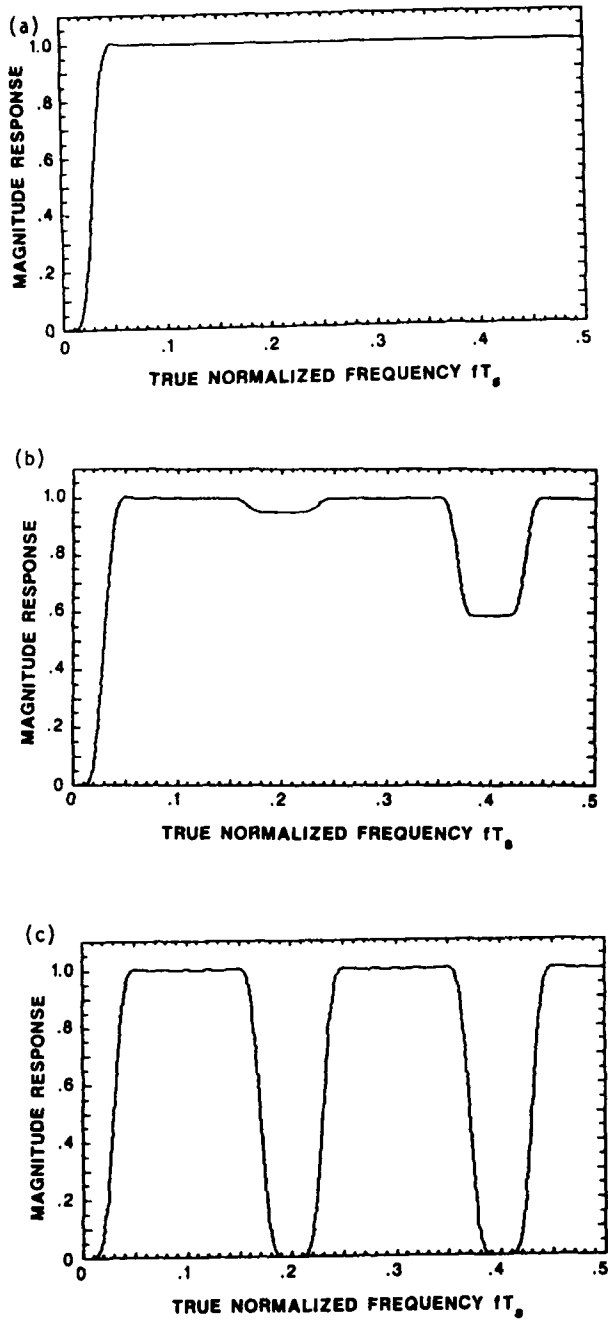

Figure 17. (a) Transfer characteristic of GCF with 101 uniformly spaced coefficients (Hamming window design with a 3 dB cutoff frequency of 0.03).

(b) Transfer characteristic of the Hamming GCF with staggered coefficients.

(c) Transfer characteristic of the Hamming GCF with 21 uniformly spaced coefficients.

notches are closely spaced because the filter has a five-times-longer sampling period $T = T_1+T_2 = (n_1+n_2)\ T_u = 5\ T_u$.

CA of both filters (from Figs. 17a,b) are given in Fig. 18. As expected, there is no appreciable decrease in CA due to staggering. This useful feature can be attributed to the design method and the properties of the window. In the case of the Chebyshev design, the weighting coefficients for uniformly spaced samples change rapidly and nonmonotonically at the beginning and end of the sequence. When several of these coefficients are dropped to create a staggered sequence, the effects on the notch become noticeable. With the Hamming window design, the coefficients change gradually and monotonically at the ends. Therefore, the extracted coefficients for the staggered sequence preserve the shape of the uniform sequence, and the effects on the notch are minimal.

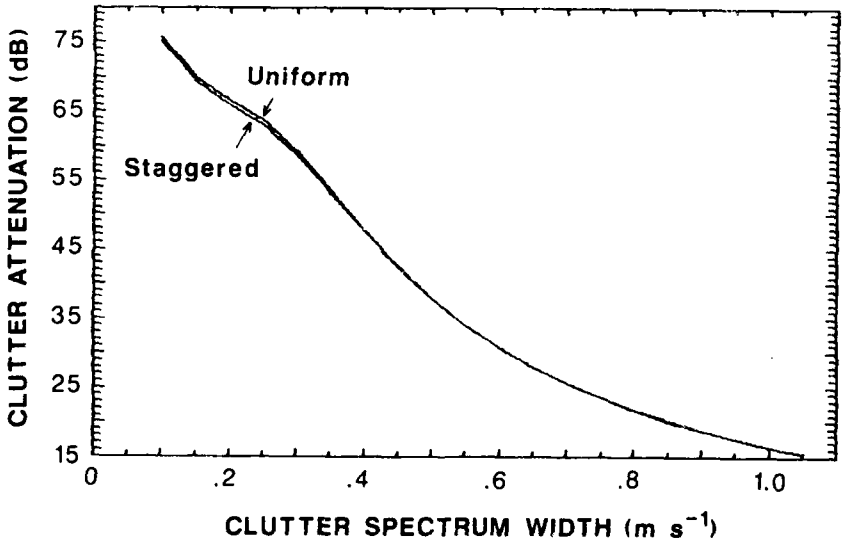

Figure 18. Clutter attenuation vs. clutter spectrum width (Hamming window design, 3 dB velocity cutoff is $v_c = 1.5$ m s^{-1} obtained from Figure 17(a) for the GCF with 101 uniformly spaced coefficients (upper curve) and the GCF with 41 staggered coefficients (lower curve).

3.5 Comparative Ground Clutter Filter (CGCF)

The transfer characteristics of the staggered PRT filter (Fig. 17b) and the split uniform PRT filter (Fig. 17c) are linear everywhere except in regions where the normalized frequency satisfies

$$fT_s = fT_2(1-K) = 0, \pm 0.2, \pm 0.4, \ldots \qquad K = T_1/T_2 = 2/3. \quad (20)$$

All nonlinearities are concentrated in narrow bands around these frequencies. It is shown in the Appendix that the nonlinearities occur at notches that are spaced by 1/T. The staggered PRT filter has a very flat amplitude characteristic (Fig. 12) but its phase (Fig. 13) is highly nonlinear in the vicinity of frequencies given by (20). This is in contrast to the transfer characteristic of the split uniform PRT filter (see Section 3.1), which has linear phase but severe attenuation in all of the notches [at frequencies given by (20)].

It is possible to detect these regions where the transfer characteristic is nonlinear by comparison of powers at the output of the staggered PRT filter with powers at the output of a split uniform PRT clutter filter. For illustration, the relationship between filter transfer functions (i.e., position of notches, etc.) is shown in Fig. 19. Note that powers will be significantly different whenever the signal is in any of the notches other than at 0 velocity. Notches near zero frequency must be well matched so that the same amount of clutter power is removed by both filters.

The pulse-pair calculation of spectral moments can be performed at the outputs of both filters and results compared in order to get redundant information. When reflectivities and mean velocities from the two filters are consistent, the result may be acceptable. When there is an inconsistency among either reflectivities or velocities, a slightly more involved decision needs to be made; one such possibility is discussed in Section 3.5.1. Because of several common elements the hardware of these two filters can be combined into one filter with two outputs. We call this combined filter a Comparative Ground Clutter Filter (CGCF).

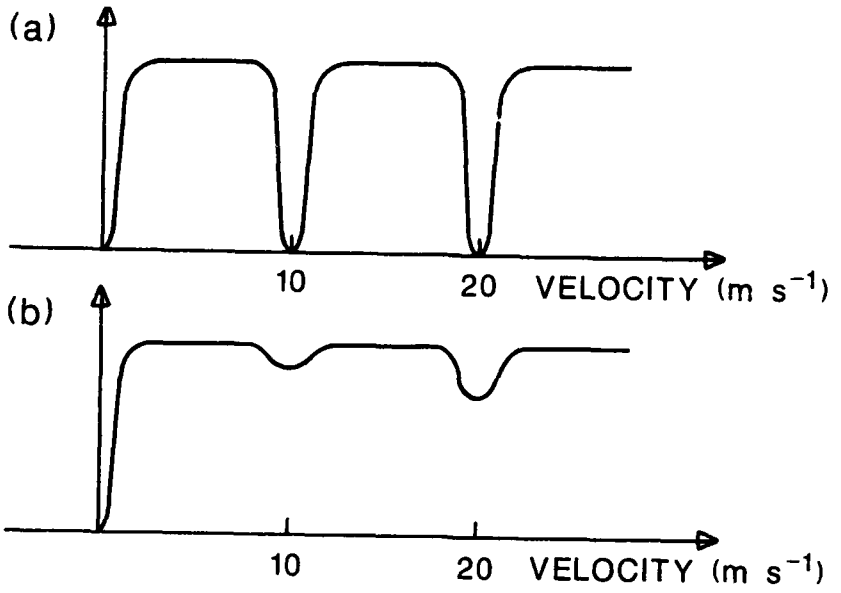

Figure 19. (a) Transfer function of a split uniform PRT ground clutter filter (see Section 3.1).

(b) Transfer function of a staggered PRT ground clutter filter (see Section 3.3).

As an example, the weighting coefficients for the low-pass part of the staggered PRT clutter filter (see Section 3.3), with an odd number of samples, are shown in Fig. 20a. Now the weighting coefficients for the low-pass part of a split uniform PRT clutter filter consist of all even number weights in Fig. 20a (i.e., ... h_{-2}, h_0, h_2...). This procedure produces well-matched filters because both sets of weighting coefficients are from the same basic window function (see Figs. 17b,c and 18).

3.5.1 Comparative ground clutter filter with binary decision logic

We present a possible solution for the CGCF filter with the decision logic in Fig. 20b. This logic is probably one of the simplest. Only two states are possible:

- signal is in one of notches
- signal is outside notches.

Signal at the output of the split uniform PRT filter is used only for power comparison with the signal from the staggered PRT filter. This signal

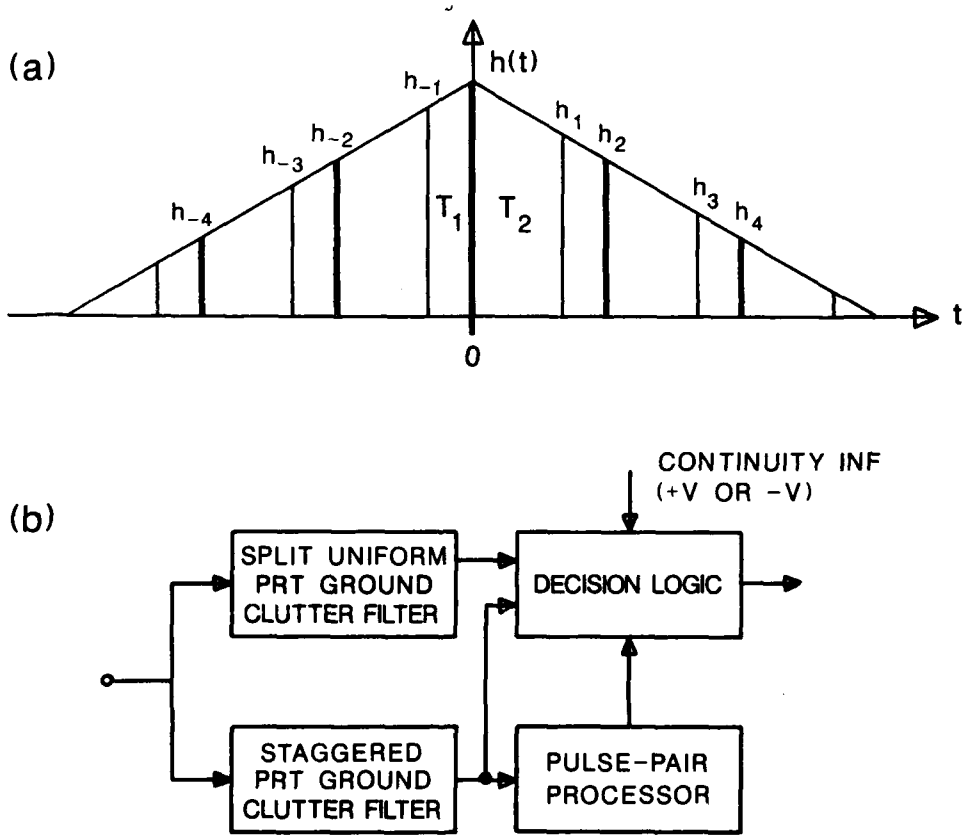

Figure 20. (a) Selection of weighting coefficients for low-pass part of a uniform PRT ground clutter filter.

(b) Diagram of the comparative ground clutter filter and decision logic.

can also be used to extract the mean velocity. For the timebeing we defray that possibility (Section 3.6) and concentrate on a simpler procedure of using only the power from that filter.

According to the transfer characteristic (Fig. 21), the velocities from the staggered PRT filter output will be confined to a fixed range of values. Thus, the velocities must be computed according to (1) in order to construct a table of decision logic Table 1.

Table 1. Decision Logic

Comparison Between Output Power	Estimated Velocity ($m\ s^{-1}$)	Chosen Velocity ($m\ s^{-1}$)
$\hat{P}_u > \hat{P}_s/\alpha^*$	$\hat{v}$	$\hat{v}$
$\hat{P}_u > \hat{P}_s/\alpha^*$	$-25 < \hat{v} < -20$	$\hat{v} = 20$ or -2
	$-20 < \hat{v} < -10$	$\hat{v} = 20$
	$-10 < \hat{v} < 0$	$\hat{v} = 20$ or -10
	$0 < \hat{v} < 10$	$\hat{v} = 10$ or -20
	$10 < \hat{v} < 20$	$\hat{v} = -20$
	$20 < \hat{v} < -25$	$\hat{v} = 20$ or -20

*$\hat{P}_u$ - Output power of the split uniform PRT filter.
$\hat{P}_s$ - Output power of the staggered PRT filter.

As before, the parameters, $\lambda = 5$ cm, $T_1 = 1$ ms, and $T_2 = 1.5$ ms are used; α is a threshold slightly larger than 1. The inequalities in the first column of Table 1 serve to establish whether the powers are close to each other; the second inequality implies that the signal is in one of the notches of the split uniform PRT ground clutter filter. Location of velocity estimates attempts to establish (albeit not uniquely) in which of the notches the signal spectrum is, so that its mean velocity can be retrieved. This is also graphically illustrated in Fig. 21a where the nonuniqueness of $\hat{v}$ that plagues this comparison is also apparent. For instance, if power comparison suggests that

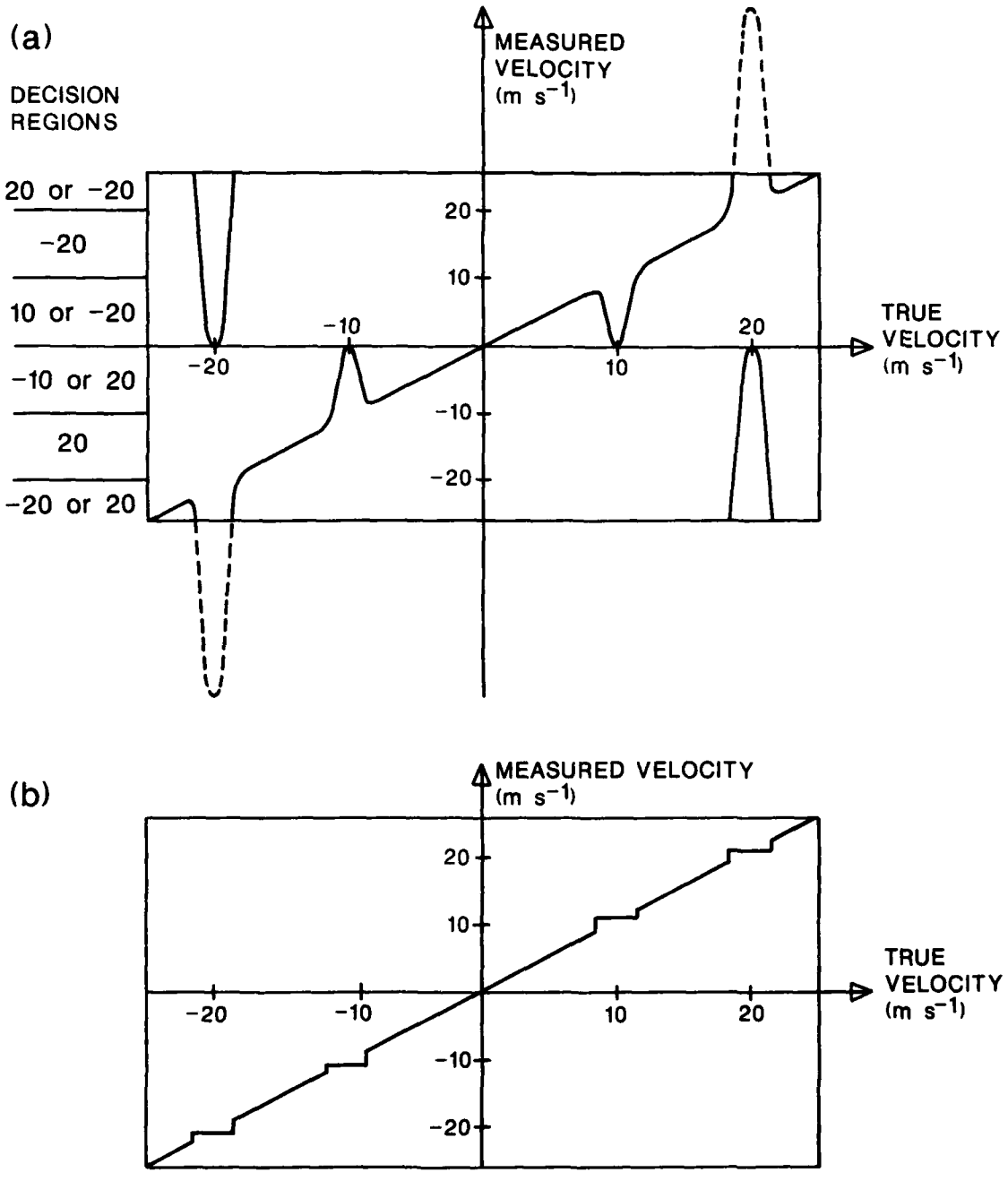

Figure 21. (a) Velocity transfer characteristic of the staggered PRT ground clutter filter. The ordinate is partitioned into decision regions used to deduce velocities lying within the notches.

(b) Velocity transfer characteristic of the comparative ground clutter filter (CGCF).

we are in a notch and the velocity estimate is 5 m s^{-1}, it is not possible to determine if the true mean velocity is 10 m s^{-1} or -20 m s^{-1}. However, the continuity of velocity fields may be used to resolve this dilemma. The overall velocity transfer characteristic, after identification of the notches, is given in Fig. 21b. We must bear in mind that the transfer in the vicinity of 0 may be misleading. Although it is linear, the signal powers will be attenuated in the notch, and therefore large errors will result.

3.6 System Simulation

In order to check some of the considered concepts and the system as a whole, we have developed a program for simulation of the weather Doppler radar signal processor. As an input signal to the processor, we have used the output from a weather signal simulation program, developed previously (Zrnic', 1975). A diagram of the simulated system is given in Fig. 22.

The weather and clutter signal are both narrowband Gaussian processes, with variable spectral width. Ground clutter has mean velocity set to 0, whereas the velocity is swept over the extended Nyquist range for the weather signal. White noise is added to both processes, and control of clutter-to-signal and signal-to-noise power is available.

The CGCF filter has two outputs: a split uniform PRT and a staggered PRT (see Section 3.5). Binary decision logic block has been explained in Section 3.5.1. It is important to realize that both outputs of the CGCF filter consist of staggered PRT's; the label, split uniform PRT on one of them, refers to the output of the split uniform PRT ground clutter filter, which is diagrammed in Fig. 3 (see Section 3.1). The pulse-pair processor performs mean frequency calculation on the outputs of CGCF. Pulse-pair processor here refers to computations of $\hat{v}$, according to Eq. (1), which includes $\hat{R}_1$ and $\hat{R}_2$. One of the outputs consists of velocities, $\hat{v}_u$, computed on staggered pulses from a split uniform PRT filter; the other is for velocities from the staggered PRT filter, which also serves as input to the decision logic. The output of the decision logic, $\hat{v}$, is the mean velocity from the pulse-pair processor, which is corrected when necessary, by the logic explained in Table 1 (see Section 3.5.1). The weighting coefficients used in the CGCF filter are from example 3 (v_c = 1.5 m s^{-1}; see Section 3.4.1). To ensure proper operation of the simulation, the outputs of all blocks have been monitored.

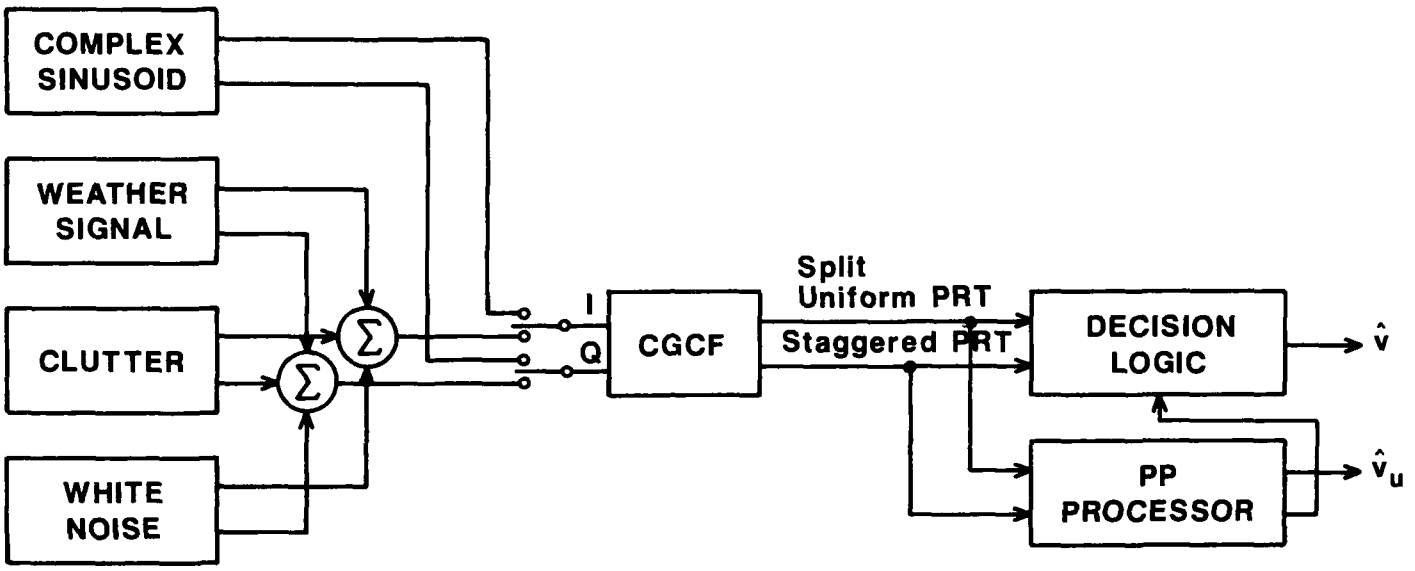

Figure 22. Diagram of system simulation.

In Fig. 23 we have plotted the measured versus true normalized Doppler shift at the output of decision logic for a pure (complex) sinusoid (see Fig. 22) that is swept over the entire extended unambiguous interval. The threshold level ($\alpha = \hat{P}_s/\hat{P}_u$) for comparison of the powers at the output of split uniform PRT and staggered PRT filter is set at $\alpha = 1.05$. The bands (at the position of notches) where the logic is active, can clearly be seen as flat segments in the input-output velocity characteristic (Fig. 23). The bias of mean velocity measurement is shown in Fig. 24. Thus we conclude that for a pure sinusoid, the input-output velocity transfer follows theoretical predictions and is satisfactory.

Next we present a more realistic situation of Gaussian-shaped weather and clutter signals. In order to obtain a precise input-output frequency transfer curve, a long time sequence with 151 uniformly spaced points was simulated. Out of 151 uniformly spaced samples, we isolated 61 staggered samples, and passed them through filters. The filter impulse response consisted of 41 samples, with a total duration of 50 ms. Therefore, the first 41 samples (out of 61) were used to load the filter (i.e., bring it into steady state) and

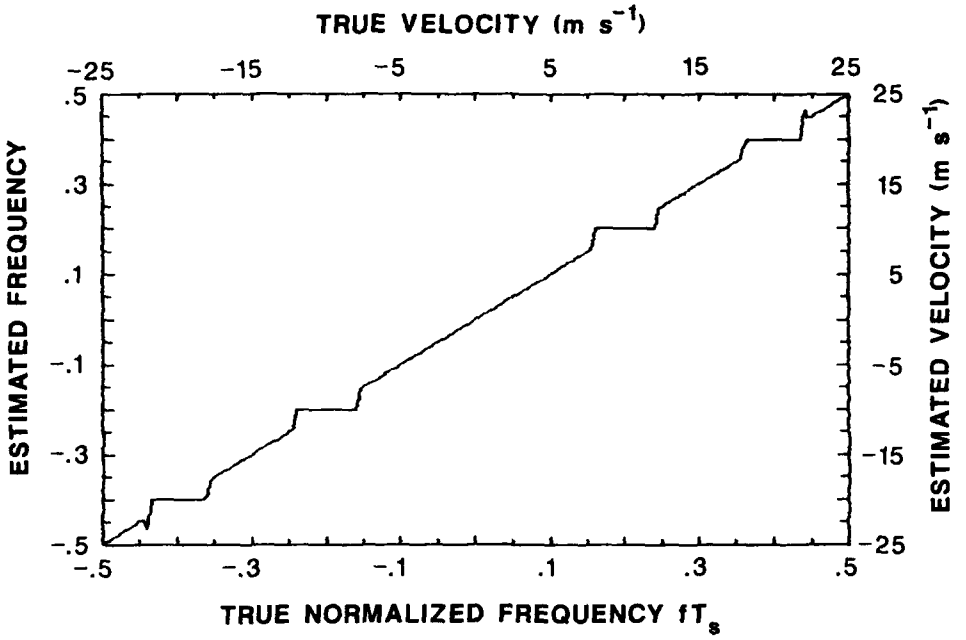

Figure 23. True vs. measured frequency for pure sinusoid signal; CGCF with decision logic (Hamming window design with cutoff frequency of 0.03).

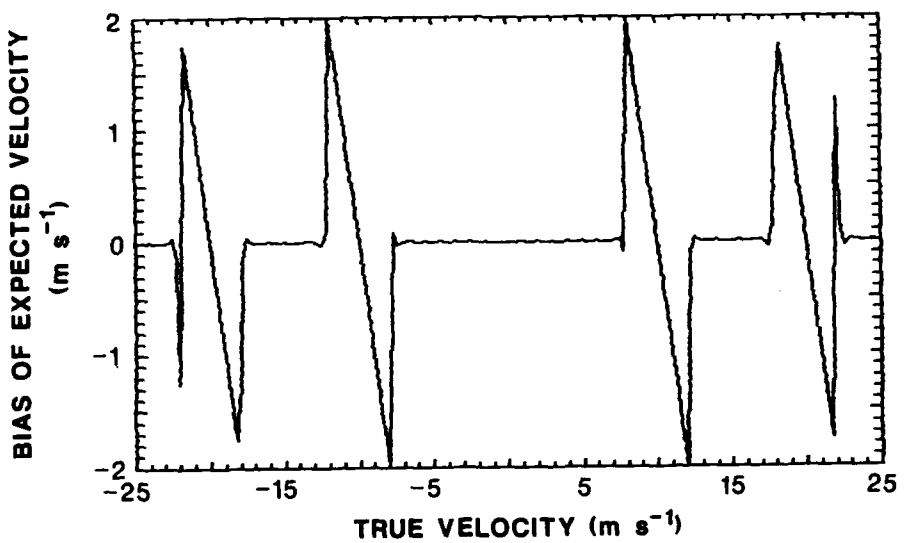

Figure 24. Mean velocity bias for a pure sinusoidal signal; CGCF with decision logic.

only the remaining 20 samples (dwell time of 25 ms) were used for calculations of $\hat{v}$ according to (1). For each input frequency (velocity) 100 different simulation trials were performed, and the output velocities were averaged to obtain transfer curves and biases. The SNR was set at 20 dB, and 101 frequency steps were used to cover the extended Nyquist interval. Several values of weather signal spectrum widths were tried. Clutter spectral width was set to 0.25 m s^{-1} and 0.5 m s^{-1}, and various ratios of signal power to clutter power (SCR) were tested. The following two cases are representative of typical results expected for weather radar.

Case 1: Clutter spectrum width σ_c = 0.25 m s^{-1}

This case, with relatively narrow clutter width, allows processing of weather signals with very low SCR (-40 dB). It follows from Fig. 18 that CA is 63 dB, and that after filtering, SCR would be 23 dB. This value of SCR is more than enough for accurate estimation of mean Doppler frequency.

In Fig. 25a, we show the estimated versus true Doppler frequency at the output of the system with binary decision logic and for a signal spectrum width σ_s = 0.25 m s^{-1} (see Section 3.5.1, CGCF filter). The bias of Doppler velocity measurement is given in Fig. 25b. The results are similar to those for a pure sinusoid and demonstrate that our concept is sound. The measured (estimated) Doppler frequencies using the output of staggered PRT filter and the output of the split uniform PRT filter (both without any decision logic) are given in Figs. 25c and 25d, respectively. Clearly the transfer is ambiguous and useless unless the decision logic is included.

Figure 26 presents the same plots as Figure 25 except that σ_s = 0.5 m s^{-1}. Figure 27 presents the same plots except that σ_s = 1 m s^{-1}. Figure 28 is the same as Fig. 27 except that σ_s = 2 m s^{-1}.

Note that the bias is mostly within acceptable limits for NEXRAD, ±2 m s^{-1}, although at larger spectrum widths there are isolated regions with larger bias.

Case 2: Clutter spectrum width σ_c = 0.5 m s^{-1}

It is expected that σ_c = 0.5 m s^{-1} is an upper limit for a 1° antenna that rotates at 5 rpm (Zrnic' and Hamidi, 1981). With this large spectrum width, CA attenuation is about 36 dB (see Fig. 18). It follows that the SCR, which can be successfully treated with this scheme, is SCR = -15 dB.

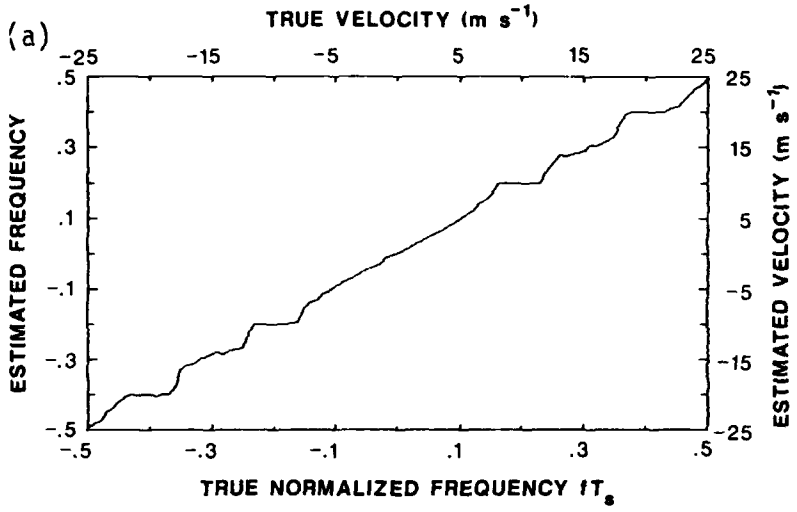

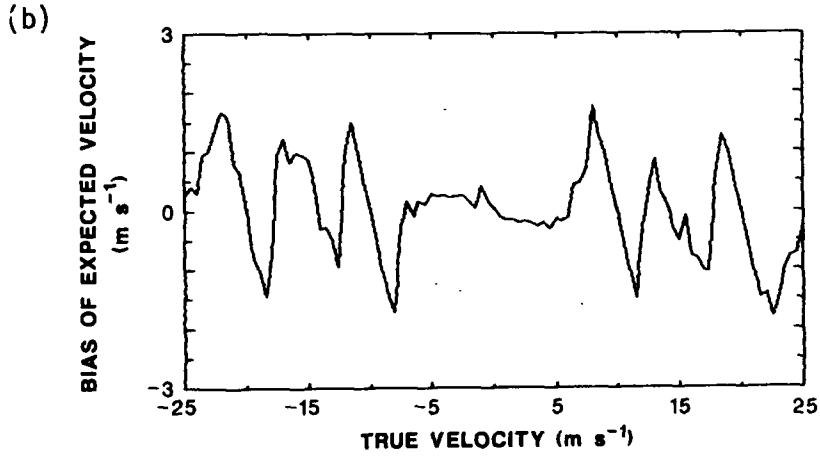

Figure 25. (a) True vs. estimated frequency for a weather signal with SCR = -40 dB, σ_s = 0.25 m s^{-1} and clutter σ_c = 0.25 m s^{-1}; CGCF with decision logic.

(b) Mean velocity bias for SCR = -40 dB, σ_s = 0.25 m s^{-1} and σ_c = 0.25 m s^{-1}; CGCF with decision logic.

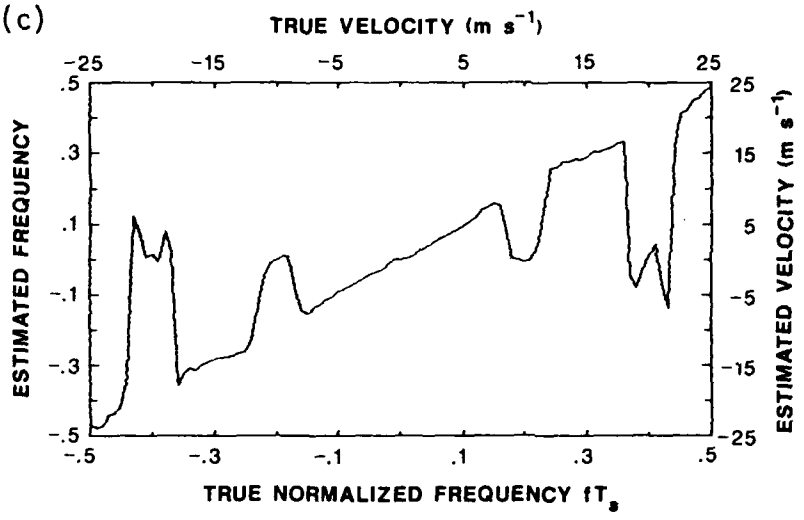

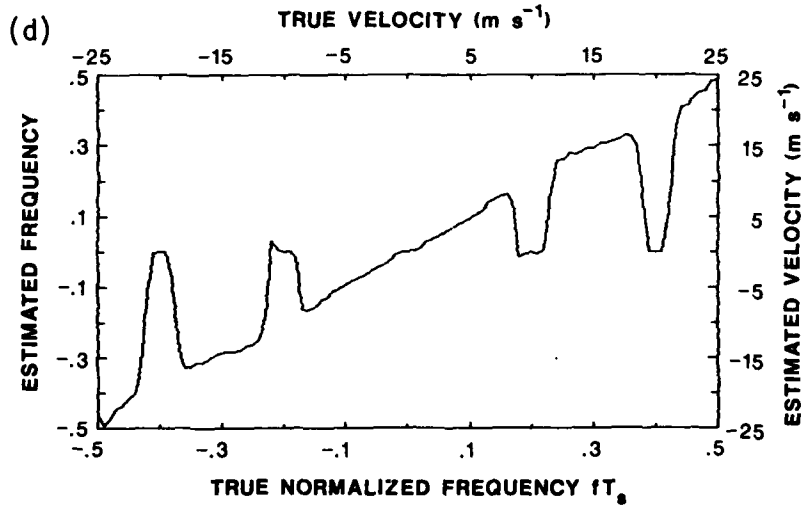

Figure 25. (c) True vs. estimated frequency at the output of the staggered PRT filter without decision logic (SCR = -40 dB, σ_c = 0.25 m s^{-1}, σ_s = 0.25 m s^{-1}).

(d) True vs. estimated frequency at the output of the split uniform PRT filter (SCR = -40 dB, σ_c = 0.25 m s^{-1}, σ_s = 0.25 m s^{-1}).

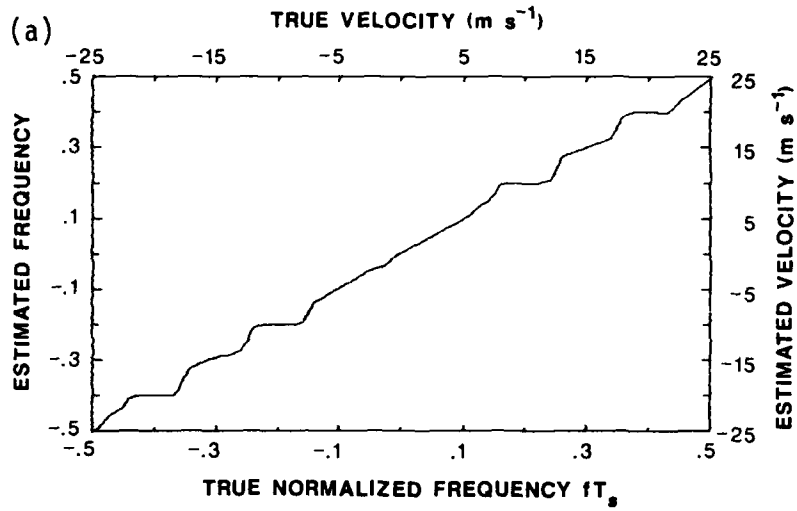

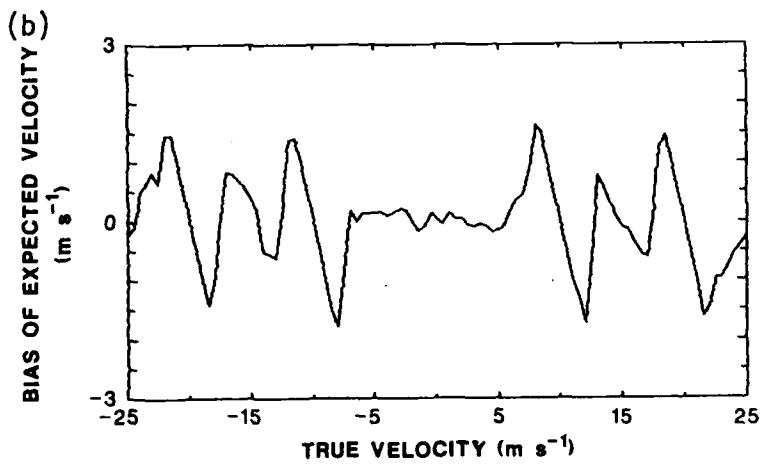

Figure 26. (a) True vs. estimated frequency (SCR = -40 dB, σ_c = 0.25 m s^{-1}, σ_s = 0.5 m s^{-1}); CGCF with decision logic.
(b) Mean velocity bias (σ_c = 0.25 m s^{-1}, σ_s = 0.5 m s^{-1}); CGCF with decision logic.

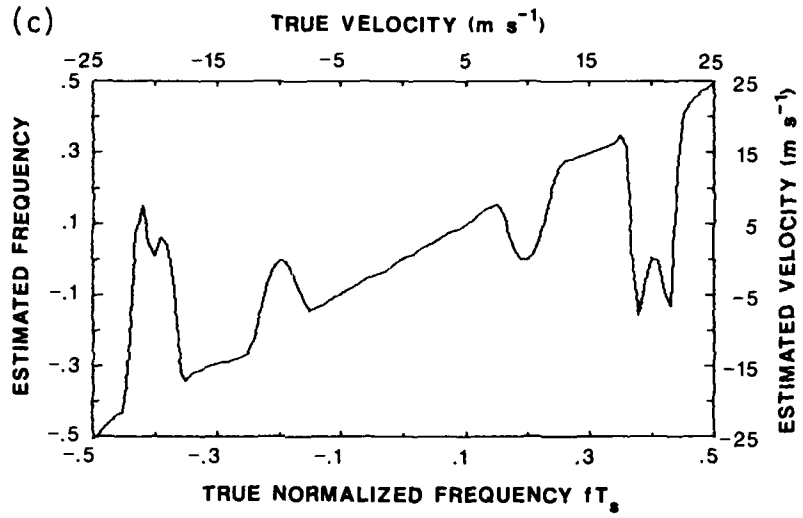

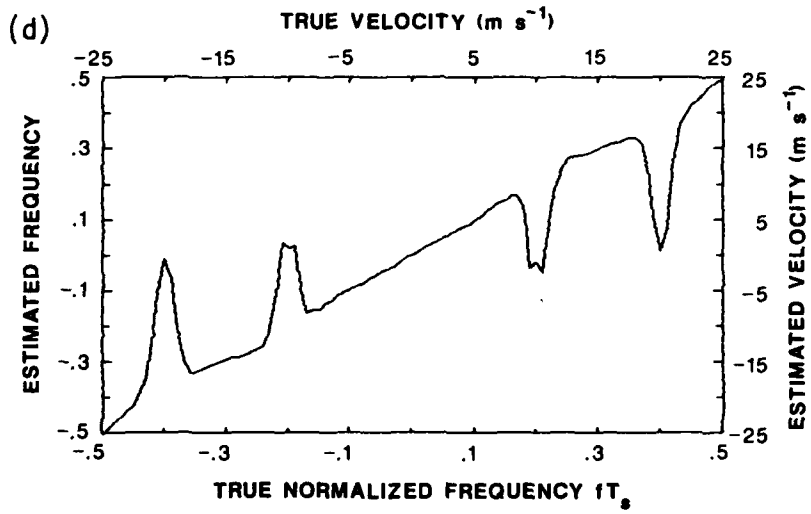

Figure 26. (c) True vs. estimated frequency at the output of the staggered PRT filter (σ_c = 0.25 m s^{-1}, σ_s = 0.5 m s^{-1}).

(d) True vs. estimated frequency at the output of the split uniform PRT filter (σ_c = 0.25 m s^{-1}, σ_s = 0.5 m s^{-1}).

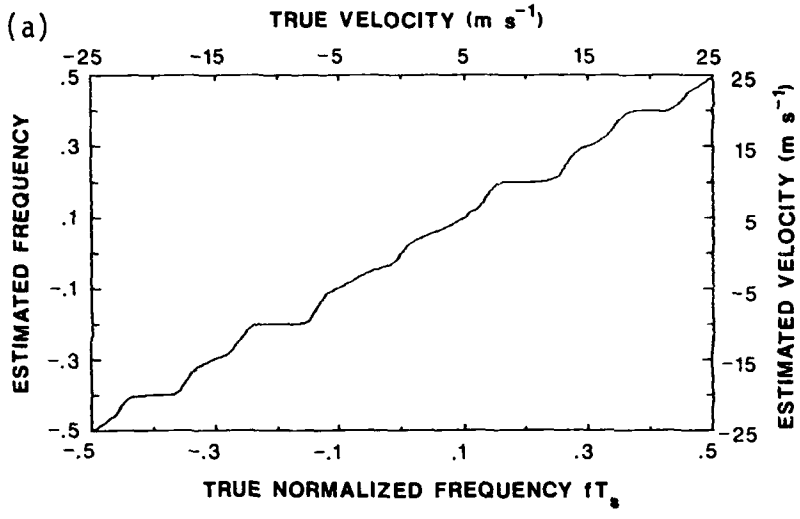

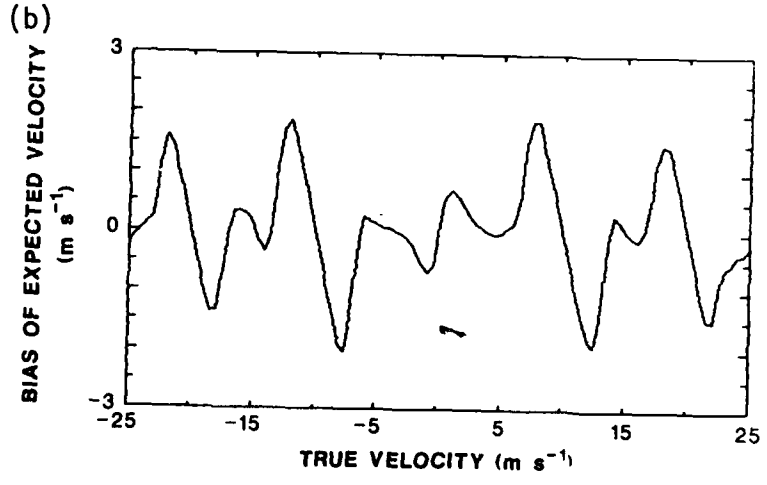

Figure 27. (a) True vs. estimated frequency (SCR = -40 dB, σ_c = 0.25 m s^{-1}, σ_s = 1 m s^{-1}); CGCF with decision logic.
(b) Mean velocity bias (σ_c = 0.25 m s^{-1}, σ_s = 1 m s^{-1}); CGCF with decision logic.

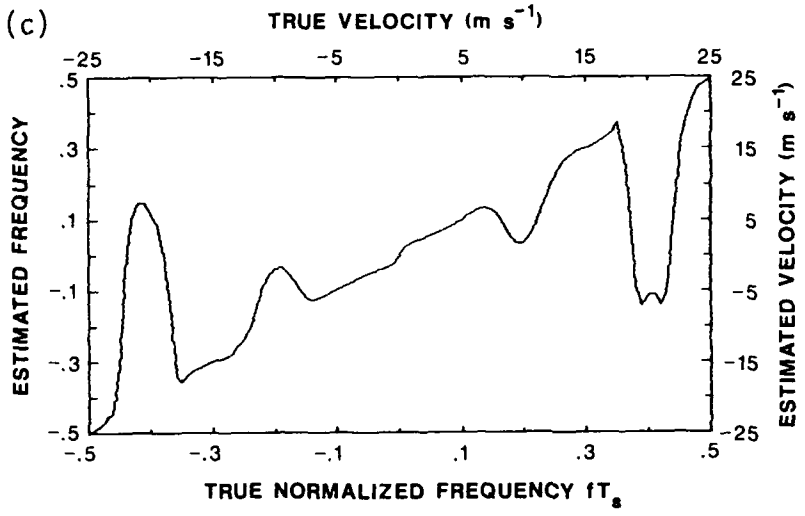

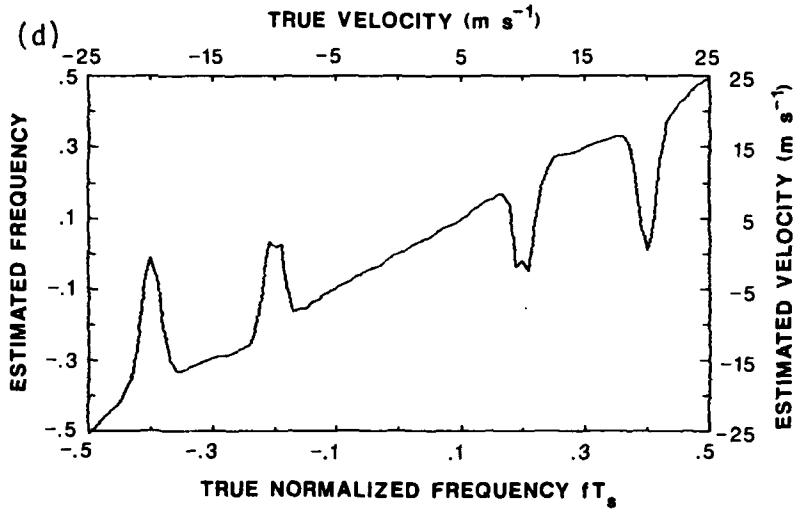

Figure 27. (c) True vs. estimated frequency at the output of the staggered PRT filter (σ_c = 0.25 m s^{-1}, σ_s = 1 m s^{-1}).

(d) True vs. estimated frequency at the output of the split uniform PRT filter (σ_c = 0.25 m s^{-1}, σ_s = 1 m s^{-1}).

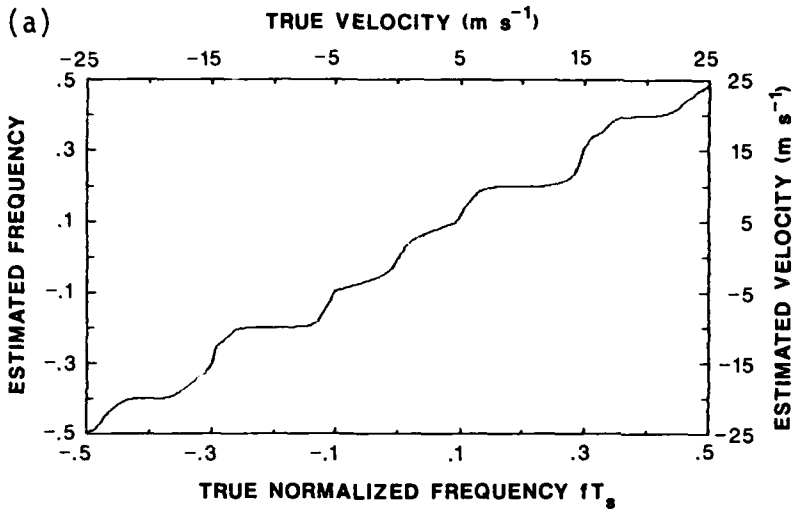

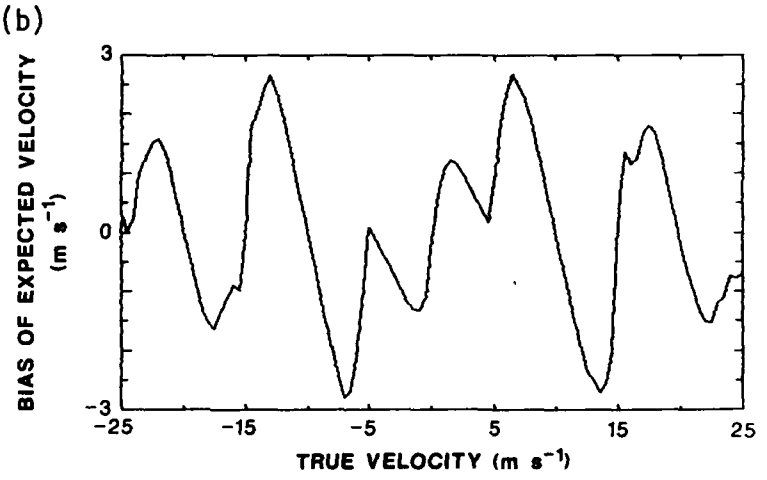

Figure 28. (a) True vs. estimated frequency (SCR = -40 dB, σ_c = 0.25 m s^{-1}, σ_s = 2 m s^{-1}); CGCF with decision logic.
(b) Mean velocity bias (σ_c = 0.25 m s^{-1}, σ_s = 2 m s^{-1}); CGCF with decision logic.

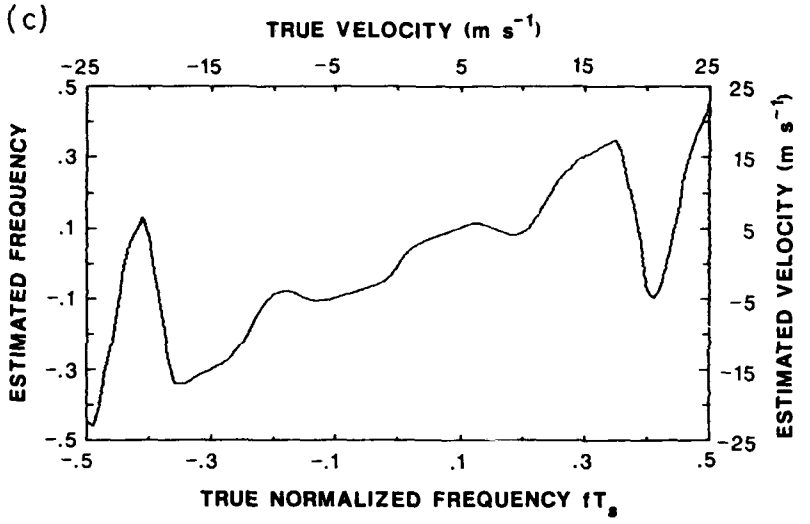

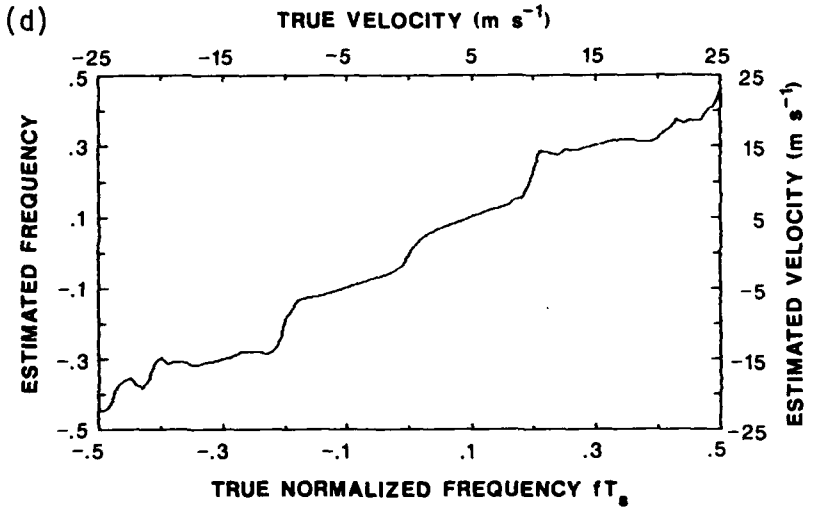

Figure 28. (c) True vs. estimated frequency at the output of the staggered PRT filter (σ_c = 0.25 m s^{-1}, σ_s = 2 m s^{-1}).

(d) True vs. estimated frequency at the output of the split uniform PRT filter (σ_c = 0.25 m s^{-1}, σ_s = 2 m s^{-1}).

In Fig. 29a we plotted the estimated versus true Doppler frequency for signal spectrum width σ_s = 0.5 m s^{-1} at the output of CGCF with decision logic (see Section 3.5.1). The Doppler velocity measurement bias is given in Fig. 29b. The estimated versus true Doppler frequency at the output of the staggered PRT filter and the split uniform PRT filter (both without any decision logic) are given in Figs. 29c and 29d, respectively.

Figure 30 is the same as Figure 29, except that σ_s = 1 m s^{-1}. Figure 31 is the same as Figure 30, except that σ_s = 2 m s^{-1}. Note that the steepness of the largest humps in Figs. 25c and 26c determines the discriminatory power of the decision logic. For velocities (frequencies) that fall on the steep part, the notch ambiguities cannot be easily resolved.

Statistical analysis

Next we briefly present errors for some of the simulations from case 1 and 2. These errors contain both the bias and random components; they are total root-mean-square errors (i.e., with respect to the true values). We have opted for the total squared error because it is rather difficult, if not impossible, to eliminate the bias, which is a function of Doppler spectrum width, mean velocity, and signal-to-clutter ratio. In Fig. 32a we have plotted the error for an SNR = 5 dB and σ_c = 0.5 m s^{-1}, σ_s = 2 m s^{-1}; almost identical results are obtained for σ_s = 1 m s^{-1}. The average error of 3 m s^{-1} is less than a theoretical prediction of 3.2 m s^{-1} (see Section 2). We stress that the theory is for an estimator without the CGCF filter, and that the decision logic has slightly reduced the errors at the location of notches. For a σ_c = 0.25 m s^{-1}, and either σ_s = 1 m s^{-1} or σ_s = 2 m s^{-1}, the errors are very similar; we show only the ones for σ_s = 1 m s^{-1} in Fig. 32b; the smaller average value of 2.6 m s^{-1} can be attributed to better filtering of the narrower clutter spectrum. Although it is satisfying that the errors are below theoretical predictions, they may still be objectionable, in which case a two-step calculation (see Section 2) or some averaging in range would be necessary. At larger SNR the errors do decrease, but not as much as expected from theory. This is shown in Figs. 32c and 32d. Note that now the SNR is 20 dB, but the average error for σ_c = 0.5 m s^{-1} and σ_s = 2 m s^{-1} is 2.3 m s^{-1}, which is much larger than the theoretically expected 0.6 m s^{-1}. This fact, together with the shape of error curves, leads us to conclude that clutter residue contributes considerably to the errors. We also expect this to be true for the two-step process, and therefore the benefits of the two-step process may

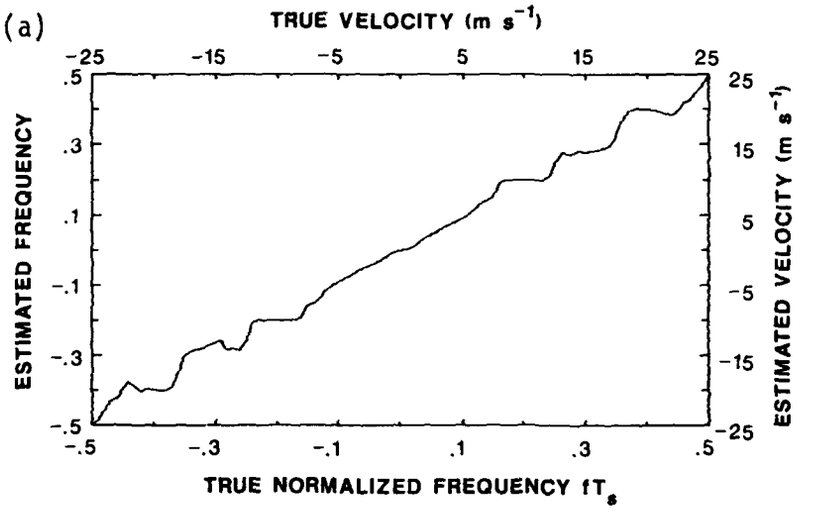

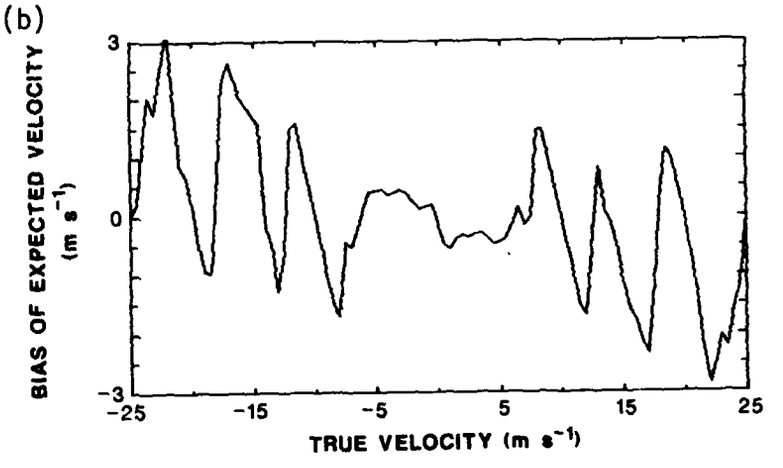

Figure 29. (a) True vs. estimated frequency (SCR = -15 dB, σ_c = 0.5 m s^{-1}, σ_s = 0.5 m s^{-1}); CGCF with decision logic.
(b) Mean velocity bias (σ_c = 0.5 m s^{-1}, σ_s = 0.5 m s^{-1}); CGCF with decision logic.

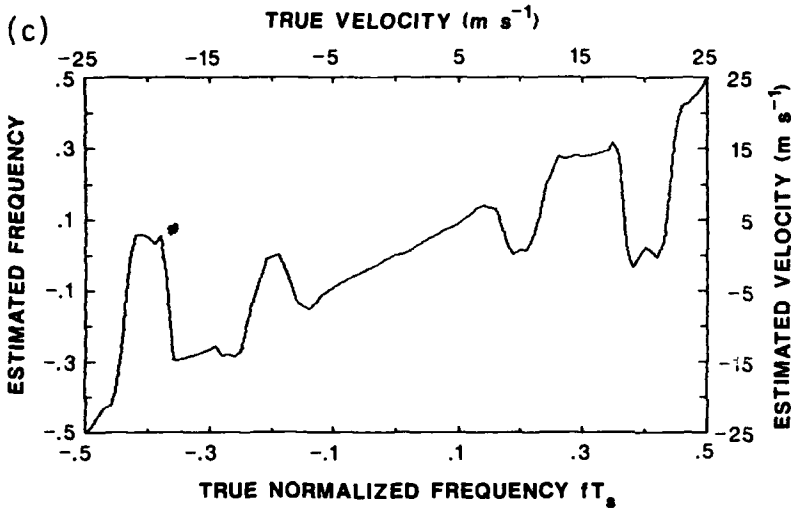

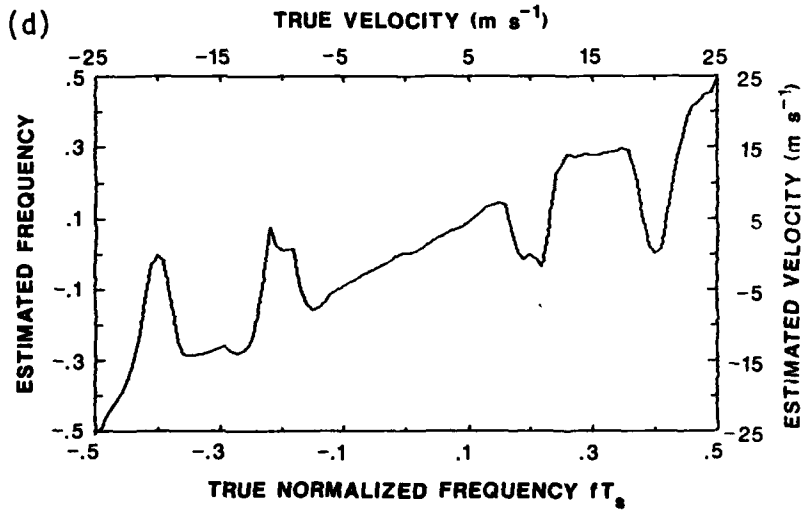

Figure 29. (c) True vs. estimated frequency at the output of the staggered PRT filter (σ_c = 0.5 m s^{-1}, σ_s = 0.5 m s^{-1}).

(d) True vs. estimated frequency at the output of the split uniform PRT filter (σ_c = 0.5 m s^{-1}, σ_s = 0.5 m s^{-1}).

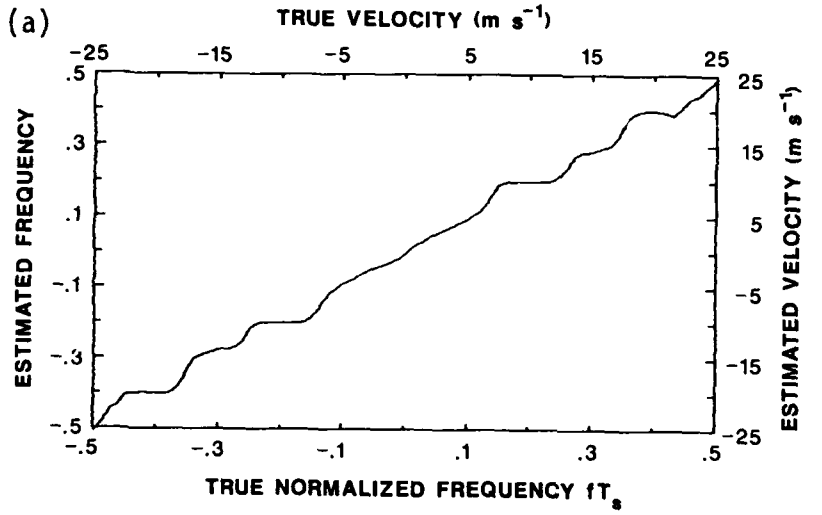

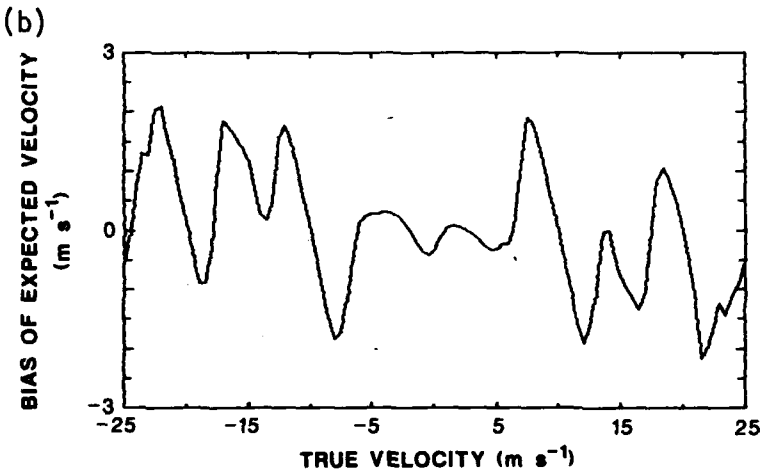

Figure 30. (a) True vs. estimated frequency (SCR = -15 dB, σ_c = 0.5 m s^{-1}, σ_s = 1 m s^{-1}); CGCF with decision logic.
(b) Mean velocity bias (σ_c = 0.5 m s^{-1}, σ_s = 1 m s^{-1}); CGCF with decision logic.

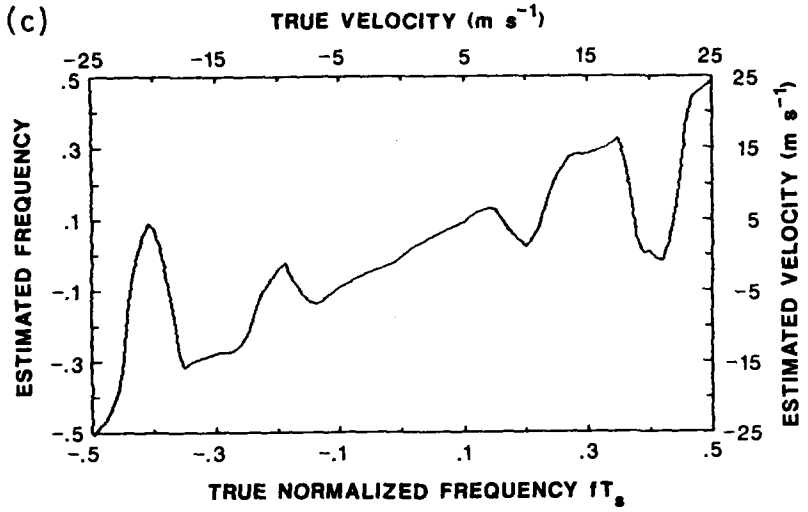

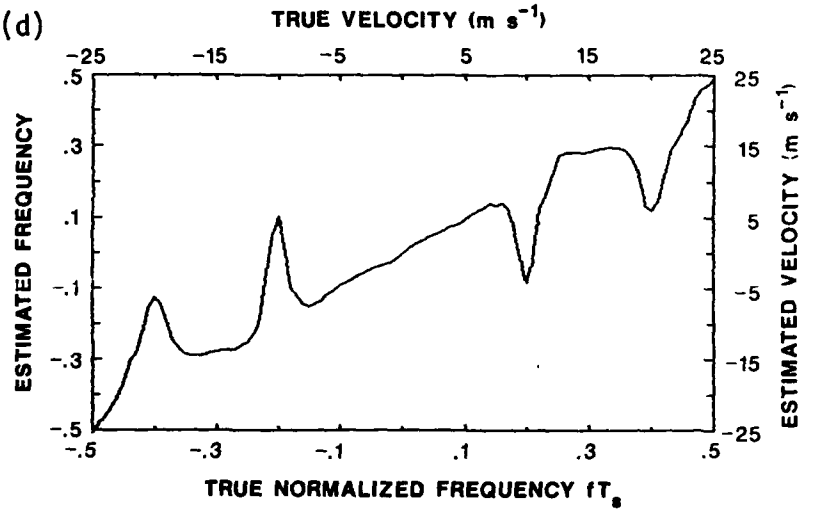

Figure 30. (c) True vs. estimated frequency at the output of the staggered PRT filter (σ_c = 0.5 m s^{-1}, σ_s = 1 m s^{-1}).

(d) True vs. estimated frequency at the output of the split uniform PRT filter (σ_c = 0.5 m s^{-1}, σ_s = 1 m s^{-1}).

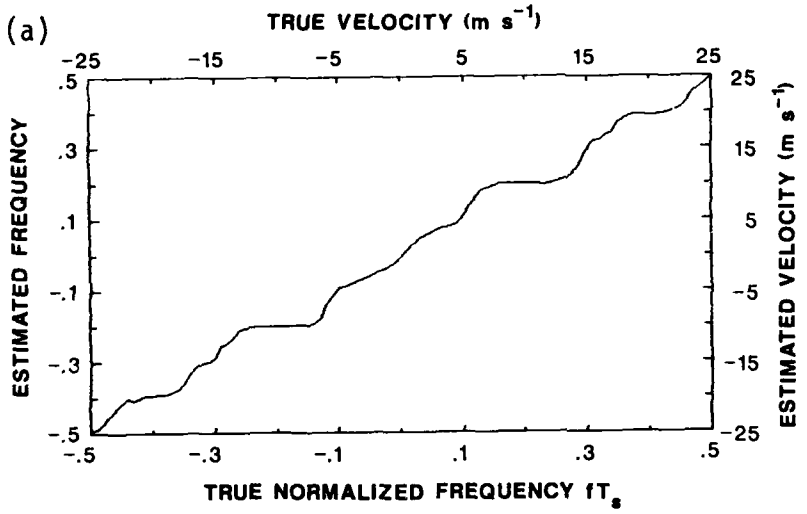

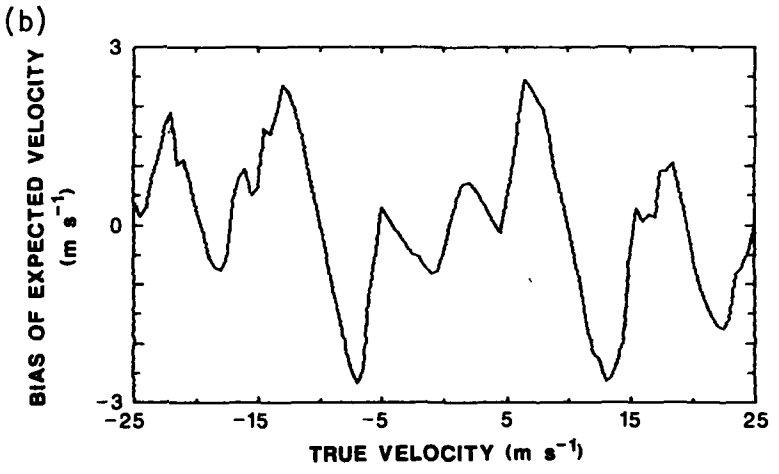

Figure 31. (a) True vs. estimated frequency (SCR = -15 dB, σ_c = 0.5 m s^{-1}, σ_s = 2 m s^{-1}); CGCF with decision logic.
(b) Mean velocity bias (σ_c = 0.5 m s^{-1}, σ_s = 2 m s^{-1}); CGCF with decision logic.

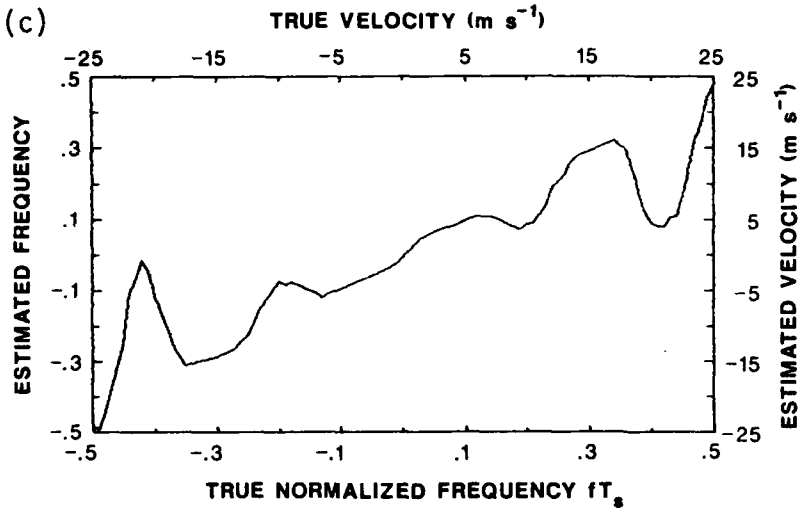

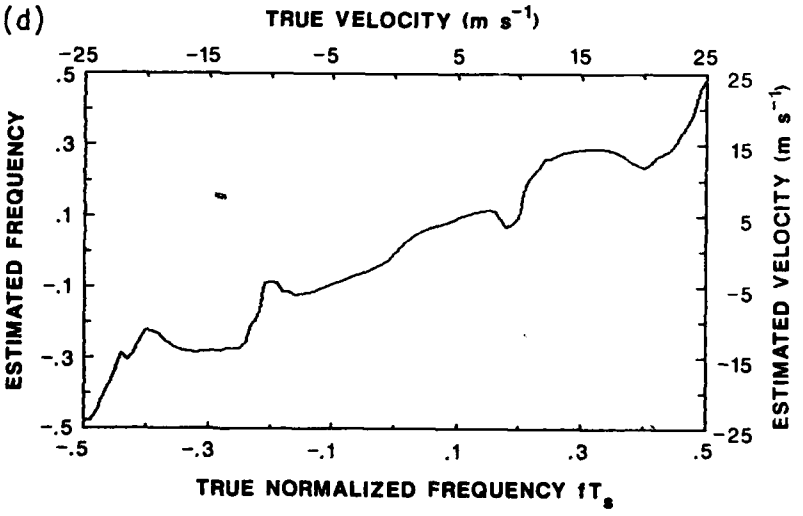

Figure 31. (c) True vs. estimated frequency at the output of the staggered PRT filter (σ_c = 0.5 m s^{-1}, σ_s = 2 m s^{-1}).

(d) True vs. estimated frequency at the output of the split uniform PRT filter (σ_c = 0.5 m s^{-1}, σ_s = 2 m s^{-1}).

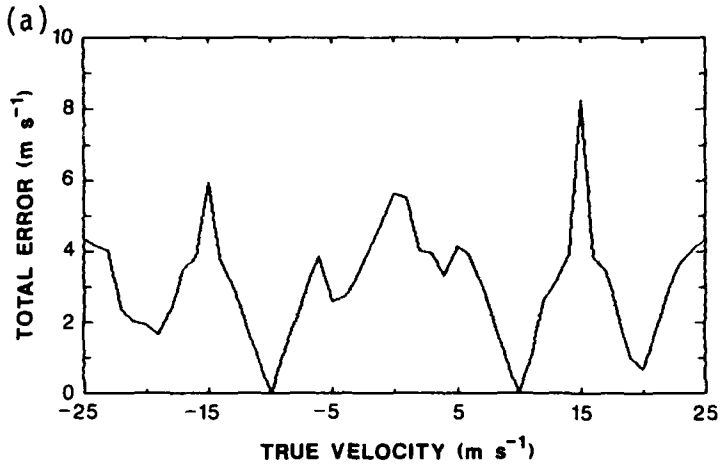

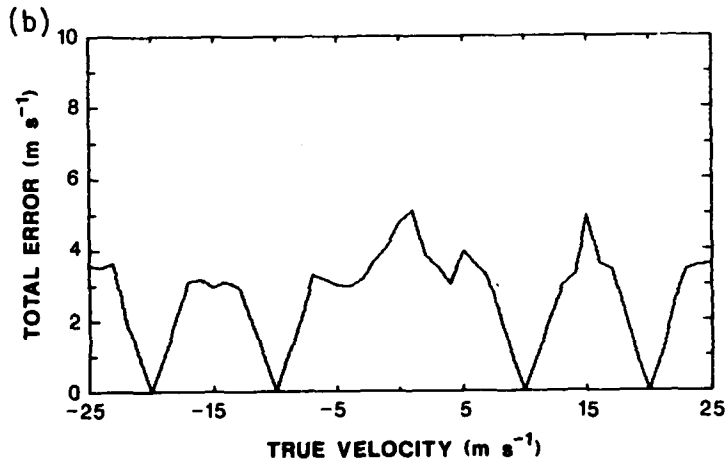

Figure 32. (a) Total root-mean-square error (bias and random) of the mean velocity estimate (CGCF with decision logic σ_c = 0.5 m s^{-1}, σ_s = 2 m s^{-1}, SNR = 5 dB, SCR = -15 dB.
(b) Same as (a) except that σ_c = 0.25 m s^{-1}, σ_s = 1 m s^{-1}, SCR = -40 dB.

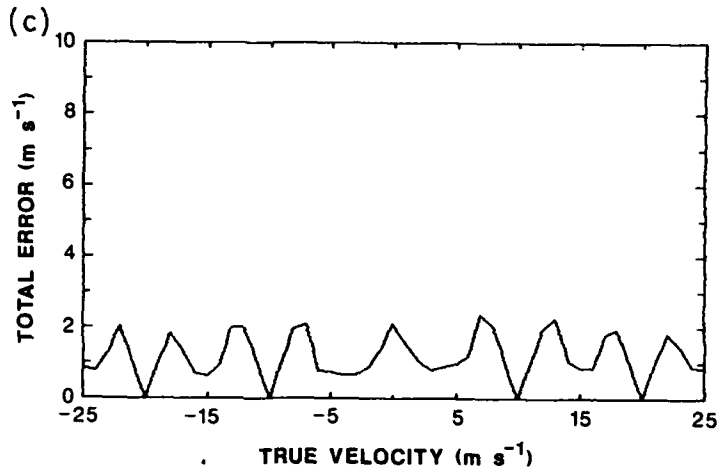

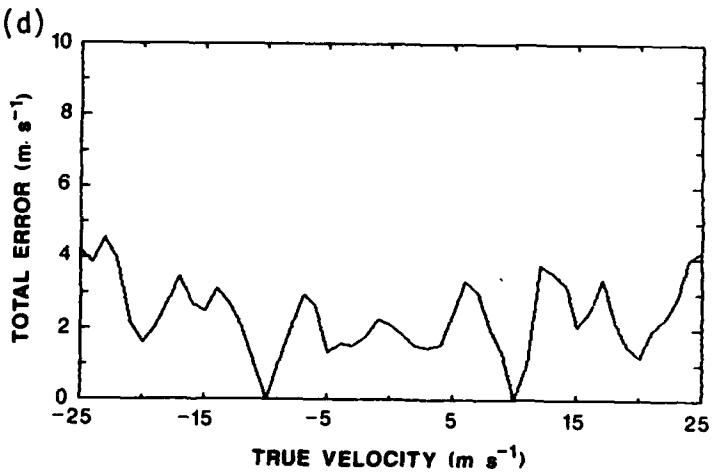

Figure 32. (c) Same as (a) except that σ_c = 0.5 m s^{-1}, σ_s = 2 m s^{-1}, SNR = 20 dB, SCR = -15 dB.

(d) Same as (a) except that σ_c = 0.25 m s^{-1}, σ_s = 1 m s^{-1}, SNR = 20 dB, SCR = -40 dB.

not be as large as suggested in Section 2, where clutter residue was not considered.

4. SUMMARY OF SIMULATION STUDIES

We simulated the input-output velocity (frequency) transfer for a stagger PRT transmission scheme with T_1 = 1 ms (v_{a1} = ± 8.3 m s^{-1}), T_2 = 1.5 ms (v_{a2} = ± 12.5 m s^{-1}) and extended unambiguous velocity v_m = ± 25 m s^{-1}. The number of staggered coefficients of the clutter filter was 41, the filter's cutoff velocity was 1.5 m s^{-1}, and the number of stagger pulses for velocity estimation was 20.

With a clutter spectrum width of 0.5 m s^{-1}, which is expected at antenna rotation rates of 5 rpm, and beamwidth of 1°, we obtain > 36 dB of clutter attenuation. However, velocities in 40% of the extended unambiguous interval require special treatment, and are subject to larger uncertainties and ambiguities. Greater clutter attenuations are possible at the expense of further increases in the region of degraded velocities; if the notch width is doubled (and σ_c = 0.5 m s^{-1}), we expect the same performance as with σ_c = 0.25 m s^{-1}, which is > 50 dB of clutter rejection.

Our simulation demonstrates that a clutter filter for staggered pulses performs according to theory, and that a decision logic is needed. The results presented do not show how often the decision logic fails, in that it wrongly identifies the notch in which the signal spectrum is located, although some idea can be obtained from the steepness of the transition region, which can be estimated in Figs. 25c through 31c. These figures suggest that signals with spectrum width of 2 m s^{-1} and larger would often yield erroneous mean velocities, if they are in some parts of the notches.

We have investigated the statistical properties of mean velocities and find the bias to be mostly below 2 m s^{-1}. This we judge to be acceptable, especially since the maxima are confined to very narrow regions of velocities.

Statistically, better overall performance may occur if the estimator (1) is used to roughly identify, within an integer multiple of $2v_{a1}$, the mean velocity. Then an improved mean velocity, $\hat{v}_1$, can be obtained from the argument of $\hat{R}_1$ (regular pulse pair or spaced pairs) which is properly dealiased with the help of $\hat{v}$. Although this has not been attempted in the present simulation, it would not change our conclusions about the ground clutter performances and the velocity transfer curves, because $\hat{v}_1$ has problems at the

same locations (notches as does $\hat{v}$. The improvement, if any, is limited by ground clutter residue, and it may not be sufficient to justify added hardware complexity.

Throughout this report we have not considered the effects of our filter on spectrum width estimation. From the distortions in the velocity transfer curves, and the fact that notches occupy about 40% of the extended unambiguous interval, we believe that the spectral widths would have significant biases through at least as much of the interval. These biases may not be correctable.

Also, our simulation did not consider the estimation of reflectivity. Because the amplitude transfer function of the staggered PRT filter is mostly flat, with a 3 dB loss in two small regions (about 20%) of the extended unambiguous interval (Fig. 17b), we conclude that reflectivity estimates from its output would be satisfactory. In relative terms, reflectivity estimates are better than velocity estimates, which are better than the spectrum width estimates.

5. CONCLUSION

The scheme developed allows ground clutter canceling on Doppler weather radars that are operating with staggered PRT's. The scheme consists of two filters that operate sequentially, so that the overall filter is time-varying with periodically changing coefficients. The filter designed by the window method produced a better overall clutter attenuation than the one based on the Chebyshev method. We have shown theoretically and through simulations that the filter would perform well (36 dB of clutter attenuation for a clutter width of 0.5 m s^{-1}) and would not degrade velocity estimates in about 60% of the extended unambiguous interval; the extended interval for example, at a wavelength of 5 cm, is 50 m s^{-1}. Forty percent of the interval is distributed into four separate frequency (velocity) bands, which require special processing to resolve possible ambiguities among them. In our example, the four-notch ambiguity is reduced (although not perfectly) by a decision logic to a two-notch ambiguity. Further resolution can be made only by invoking auxiliary information such as spatial continuity.

Magnitude transfer curves of the filter suggest that reflectivity estimates would be very satisfactory, but the spectrum width estimates may have degradation in the form of practically uncorrectable biases. Simulations show

that mean velocities obtained after clutter filtering have errors < 2.3 m s^{-1} if SNR's are 20 dB or larger. At lower SNR's (e.g., 5 dB) the average errors are less than 3.2 m s^{-1}, but peak errors in narrow velocity bands can be as large as 7 m s^{-1}. These errors are larger than the specification (1 m s^{-1}) for the TDWR.

Because of the complicated hardware and less than spectacular clutter canceling, the staggered PRT scheme must be carefully weighed against a simpler random phase procedure (Zrnic' and Mahapatra, 1985). If the main goal is to survey weather over a very limited area, such as an airport, then a uniform PRT (i.e., a random phase scheme) can usually be found such that the first trip echo is not obscured by out-of-trip echoes. Perhaps the staggered PRT scheme should be used only for surveillance of weather over larger areas farther from the radar, where clutter problems are not significant.

APPENDIX

POSITION OF NOTCHES IN A LOW-PASS FILTER USED FOR STAGGERED PULSE FILTER

Consider a staggered pulse train and a low-pass filter to extract ground clutter. Let us assume that the filter is a simple moving average consisting of 2M samples. Its transfer function evaluated from two geometric progressions is as follows:

$$H(\omega) = \frac{1}{2M} \cdot \frac{\sin M\omega T/2}{\sin \omega T/2} \cdot (1 + e^{j\omega T_1}) \cdot e^{j\omega T(M-1)/2}$$

where, as before, $T = T_1 + T_2$.

This filters' passband will be centered at zero frequency, and it will also have enhanced transfer at ±1/T, ±2/T, etc. Only when $T_1 = T_2$ (i.e., the pulses are not staggered) will the transfer be enhanced at ±2/T, ±4/T, etc., locations that are 2 times farther removed from zero. But this latter case is of no practical use. It is the staggered train that can help reduce ambiguities, and we see that a low-pass filter for such a train has repeated peaks that are not sufficiently removed from zero. In our example of T = 2.5 ms, the peaks are at ±10 m s^{-1}, ±20 m s^{-1}, etc. Now, when filtered clutter is subtracted from the original pulse train, weather echo signals that are centered at the peaks of the low-pass filter would also be removed. Thus, notches are located at ±1/T, ±2/T, etc. Other standard, but nonuniform, weights will also create similar notches. Complete elimination of such notches would also result in the elimination of the notch at zero frequency.

Because there is no way to eliminate the notches completely without also eliminating the notch at zero frequency, we have decided to take advantage of the known position of the notches in developing the logic for the comparative ground clutter filter (see Section 3.5).

REFERENCES

Doviak, R.J., and D.S. Zrnic', 1984: Doppler Radar and Weather Observations. Academic Press, Orlando, Florida, 458 pp.

Doviak, R.J., D. Sirmans, D.S. Zrnic', and G.B. Walker, 1978: Considerations for Pulse-Doppler Radar Observations of Severe Thunderstorms. J. Appl. Meteorol., 17, 189-205.

DFDP (Digital Filter Design Pack for TI TMS 32010), 1985: Ver. 1.10, Atlanta Signal Processing, Inc., Atlanta, Georgia.

Evans, J.E., 1983: Ground Clutter Cancellation for the NEXRAD System. MIT Lincoln Lab Report ATC-122.

Chornoboy, E., 1988: Personal Communication.

Rabiner, L.R., and B. Gold, 1975: Theory and Application of Digital Signal Processing, Prentice Hall, Inc., Englewood Cliffs, New Jersey.

Sirmans, D., D.S. Zrnic', and W. Bumgarner, 1976: Extension of maximum unambiguous Doppler velocity by use of two sampling rates. **Preprints**, 17th Conf. Radar Meteorology, American Meteorological Society, pp. 23-28.

Zrnic', D.S., 1975: Simulation of weatherlike Doppler spectra and signals. Journal of Applied Meteorology, Vol. 14, No. 4, June 1975, pp. 619-620.

Zrnic', D.S., 1977: Spectral moment estimates from correlated pulse pairs. IEEE Trans. Aerosp. Electron. Syst., AES-13, 344-354.

Zrnic', D.S., 1979: Estimation of spectral moments for weather echoes. IEEE Trans. Geosci. Electronics, GE-15(5), 613-619.

Zrnic', D.S., and S. Hamidi, 1981: Consideration for the Design of Ground Clutter Cancellers for Weather Radar. FAA Report No. DOT/FAA/RD-81/72.

Zrnic', D.S., and P. Mahapatra, 1985: Two methods for ambiguity resolution in pulse Doppler weather radars. IEEE Trans. Aerosp. Electron. Syst., AES-21, 470-483.

END

6-89

DTIC